AMERICAN SOCIETY FOR MICROBIOLOGY | Infection and Immunity®

BACTERIAL INFECTIONS

Identification of Two Variants of *Acinetobacter baumannii* Strain ATCC 17978 with Distinct Genotypes and Phenotypes

Christiaan D. M. Wijers,[a,b] Ly Pham,[a,b] Swapna Menon,[c] Kelli L. Boyd,[a,b] Hannah R. Noel,[d] Eric P. Skaar,[a,b] Jennifer A. Gaddy,[a,b,e,f] Lauren D. Palmer,[d] Michael J. Noto[a,b,e]

[a]Department of Pathology, Microbiology, and Immunology, Vanderbilt University Medical Center, Nashville, Tennessee, USA
[b]Vanderbilt Institute for Infection, Immunology, and Inflammation, Vanderbilt University Medical Center, Nashville, Tennessee, USA
[c]AnalyzeDat Consulting Services, Ernakulam, Kerala, India
[d]Department of Microbiology and Immunology, University of Illinois Chicago, Chicago, Illinois, USA
[e]Department of Medicine, Vanderbilt University Medical Center, Nashville, Tennessee, USA
[f]Department of Veterans Affairs, Tennessee Valley Healthcare Systems, Nashville, Tennessee, USA

ABSTRACT *Acinetobacter baumannii* is a nosocomial pathogen that exhibits substantial genomic plasticity. Here, the identification of two variants of *A. baumannii* ATCC 17978 that differ based on the presence of a 44-kb accessory locus, named AbaAL44 (*A. baumannii* accessory locus 44 kb), is described. Analyses of existing deposited data suggest that both variants are found in published studies of *A. baumannii* ATCC 17978 and that American Type Culture Collection (ATCC)-derived laboratory stocks comprise a mix of these two variants. Yet, each variant exhibits distinct interactions with the host *in vitro* and *in vivo*. Infection with the variant that harbors AbaAL44 (*A. baumannii* 17978 UN) results in decreased bacterial burdens and increased neutrophilic lung inflammation in a mouse model of pneumonia, and affects the production of interleukin 1 beta (IL-1β) and IL-10 by infected macrophages. AbaAL44 harbors putative pathogenesis genes, including those predicted to encode a type I pilus cluster, a catalase, and a cardiolipin synthase. The accessory catalase increases *A. baumannii* resistance to oxidative stress and neutrophil-mediated killing *in vitro*. The accessory cardiolipin synthase plays a dichotomous role by promoting bacterial uptake and increasing IL-1β production by macrophages, but also by enhancing bacterial resistance to cell envelope stress. Collectively, these findings highlight the phenotypic consequences of the genomic dynamism of *A. baumannii* through the evolution of two variants of a common type strain with distinct infection-related attributes.

KEYWORDS *Acinetobacter*, host-pathogen interactions, pathogenesis, variable phenotypes

Acinetobacter baumannii is a Gram-negative, opportunistic pathogen that is a common cause of infections such as pneumonia, wound infections, and sepsis (1–3). Infections with *A. baumannii* are often severe, and mortality rates associated with *A. baumannii* pneumonia are as high as 60% (4, 5). Further complicating infections with *A. baumannii* is the emergence of multidrug resistant (MDR) isolates. Isolates resistant to aminoglycosides (6–8), carbapenems (9–12), and the last-resort antibiotic colistin (13–17) have emerged as the causative agents of human disease over the last few decades. Panresistant strains of *A. baumannii* that are resistant to all clinically available antimicrobials are also encountered at an increased frequency (18, 19). Because of this, the Centers for Disease Control and Prevention have indicated carbapenem-resistant *A. baumannii* as an urgent threat (20). Studies of antibiotic-resistant *A. baumannii* primarily rely on clinical isolates (21, 22), whereas studies of bacterial pathogenesis and

Citation Wijers CDM, Pham L, Menon S, Boyd KL, Noel HR, Skaar EP, Gaddy JA, Palmer LD, Noto MJ. 2021. Identification of two variants of *Acinetobacter baumannii* strain ATCC 17978 with distinct genotypes and phenotypes. Infect Immun 89:e00454-21. https://doi.org/10.1128/IAI.00454-21.

Editor Andreas J. Bäumler, University of California, Davis

Address correspondence to Michael J. Noto, michael.james.noto@emory.edu.

Received 12 August 2021
Accepted 19 August 2021
Accepted manuscript posted online 30 August 2021
Published 16 November 2021

infection biology often rely on type strains. Type strains are descendants of the original isolates that exhibit all of the relevant phenotypic and genotypic properties cited in the original published taxonomic circumscriptions (23). Strains 17978, 19606, and AB5075 are examples of type strains used to study *A. baumannii* pathogenesis. *A. baumannii* 17978 was isolated in 1951 from an infant with meningitis and is susceptible to most antibiotics (24), *A. baumannii* 19606 was isolated in 1948 from the urine of a patient with a urinary tract infection (25), and *A. baumannii* AB5075 was isolated in 2008 from the tibia of a patient with osteomyelitis (26). These type strains have been used to identify *A. baumannii* genes required for persistence in the lung and to study *A. baumannii* virulence factors (26–33).

Strains of *A. baumannii* exhibit genomic plasticity through the incorporation and loss of genetic material (2, 34), underscored by genomic analyses of *A. baumannii* that have revealed an unusually large number of "singleton" genes that are unique to a given strain of *A. baumannii* and do not occur in other strains (35). The majority of exogenous genetic material incorporated by *A. baumannii* constitutes antibiotic resistance genes (36–38), selected for in part by the use of antimicrobials in health care settings (39, 40). This suggests that gene acquisition contributes to the emergence of MDR isolates of *A. baumannii*. Gene loss also contributes to differential patterns of antimicrobial resistance among *A. baumannii*, as a partial deletion of Tn*1548* in *A. baumannii* ABUH315100 resulted in the deletion of the *armA* amikacin resistance gene (21). *A. baumannii* genomic plasticity also facilitates changes that affect virulence and interactions with its environment, including competing bacteria and health care settings (36). For instance, disruption of the *gtr6* gene by spontaneous transposon (Tn) insertion eliminates a branch point in the capsular carbohydrate structure of the clinical isolate HUMC1 and renders it hypervirulent in a mouse model of bacteremia (41). Furthermore, several MDR strains of *A. baumannii* have acquired the plasmid pAB3 and related plasmids, which harbor multiple antibiotic resistance genes and encode repressors of the *A. baumannii* type 6 secretion system (T6SS), which can be used to directly kill competing bacteria (42, 43). Other clinical isolates of *A. baumannii* have lost genes encoding the T6SS (38, 44). This suggests that subpopulations of *A. baumannii* that have lost T6SS genes or harbor pAB3 have a competitive advantage in environments where antibiotics are present, such as health care facilities. In contrast, subpopulations of *A. baumannii* that harbor T6SS genes and lack pAB3 are able to actively attack competing bacteria.

Here, the identification of two variants of *A. baumannii* ATCC 17978 is described. These variants have been used interchangeably in pathogenesis studies but differ by the presence of an accessory locus and have unique attributes when interacting with host factors both *in vitro* and *in vivo*.

RESULTS

Two common variants of *A. baumannii* ATCC 17978 differ by the presence of an accessory genetic locus and by multiple single-nucleotide polymorphisms. During investigations into the genetic determinants of *A. baumannii* pathogenesis using a Tn*5* transposon mutant library of *A. baumannii* 17978, conserved phenotypes were observed among several transposon (Tn) mutants containing insertions into unrelated genes. In a macrophage model of *A. baumannii* infection, murine bone marrow-derived macrophages (BMDMs) produced differential quantities of the proinflammatory cytokine IL-1β upon infection with multiple Tn mutants than when infected with wild-type (WT) *A. baumannii* 17978 (see Fig. S1A in the supplemental material). In addition, phenotypic profiling of these mutants using scanning electron microscopy (SEM) revealed the presence of pili on the surface of multiple Tn mutants but not on the WT strain (Fig. S1B and C). As the Tn*5* library had been constructed at a different institution, the finding of conserved phenotypes among multiple Tn insertion mutants raised concern that the parental *A. baumannii* 17978 variant used for library construction differed from the *A. baumannii* 17978 variant used as a comparator for the BMDM infection and SEM experiments. To test this hypothesis, the genome sequences of the parental variant used for library construction (*A. baumannii* 17978 UN) and of the variant used as the comparator in the BMDM infection and SEM assays (*A. baumannii* 17978 VU) were

TABLE 1 Summary data for two variants of *A. baumannii* 17978[a]

Characteristic or descriptor	Variant of *A. baumannii* 17978	
	VU	UN
Accession no. for NCBI reference genome(s), chromosome (source or reference)	NZ_CP018664 (104); CP012004 (42)	CP079931 (this study)
UIC lab stock composition (no. of colonies/total no. of colonies)[b]	1/36	35/36
VUMC lab stock composition (no. of colonies/total no. of colonies)[c]	2/6	4/6
No. of bases	4,066,914	4,100,908
No. of genes	3,910	3,938
Avg nucleotide identity (%)	99.99	99.99
AbaAL44	Absent	Present
IS701-like IS*Aba11* family transposase upstream of *pitA_2*	Absent	Present
IS*Aba18* downstream of *ACX60_00585*	Present	Absent

[a]Single-nucleotide polymorphisms are shown in Table S3 in the supplemental material.
[b]ATCC 2021.
[c]ATCC 2009.

determined by PacBio sequencing (45). Structural comparison of these genomes revealed several differences, including differences in the size of the genomes, as well as different locations of an IS*701*-like element within each genome (Table 1). Notably, the genome of *A. baumannii* 17978 UN contained a 44-kb locus, encompassing multiple accessory genes, that was not present in the genome of *A. baumannii* 17978 VU (Table 1, Fig. 1A, and Table S2). This locus was named AbaAL44 (*Acinetobacter baumannii* accessory locus 44 kb). The accessory genes present within AbaAL44 include putative biosynthesis genes, transcriptional regulators, and genes associated with replication, as well as several putative bacterial pathogenesis genes. AbaAL44 includes *smf-1*, *yadV*, *htrE*, and *mrkD*, which together are predicted to encode a type I pilus or fimbriae; a gene predicted to encode a catalase (*KZA74_09300*); and a gene predicted to encode a cardiolipin synthase (*clsC2*) (Fig. 1A and Table S2). Additional genetic differences between *A. baumannii* 17978 UN and 17978 VU variants including single-nucleotide polymorphisms (SNPs), are shown in Table S3.

The identification of two variants of *A. baumannii* ATCC 17978 within a laboratory raised the possibility that these two variants are present in other research laboratories. AbaAL44 is present in the *A. baumannii* 17978 genome published by the American Type Culture Collection (ATCC) in 2019 (https://genomes.atcc.org/genomes/e1d18ea4273549a0), but absent in two other *A. baumannii* 17978 reference genomes available in the NCBI database (accession numbers NZ_CP018664 and CP012004; see Table 1), indicating that both *A. baumannii* 17978 VU and 17978 UN variants are represented among the published *A. baumannii* genomes. Frozen stocks of *A. baumannii* ATCC 17978 obtained from ATCC in 2009 and a different stock obtained in 2021 were streaked for individual colonies, which were screened using PCR for the presence of the accessory cardiolipin synthase gene (*clsC2*) included in AbaAL44. The accessory gene *clsC2* was present in 4 out of 6 colonies screened from the 2009 laboratory stock and in 35 out of 36 colonies screened from the 2021 laboratory stock, demonstrating that these culture collection stocks included a mixed population of *A. baumannii* 17978 variants VU and UN (Table 1 and Fig. 1B). To provide a high-quality reference genome, we performed Nanopore long-read sequencing on *A. baumannii* 17978 UN, isolated from an ATCC stock in 2021 (NCBI accession numbers CP079931, CP079932, CP079933, and CP079934; see Table 1). Illumina sequencing of *A. baumannii* 17978 UN isolates from 2009 and 2021 laboratory stocks found no predicted mutations compared to this new 17978 UN reference genome. These data indicate that the *A. baumannii* 17978 UN and 17978 VU variants differ from one another at a genetic level and that at least two ATCC-derived laboratory stocks of *A. baumannii* 17978 include these variants.

***A. baumannii* 17978 VU and 17978 UN variants exhibit differential pathogenicity in a mouse model of pneumonia.** *A. baumannii* 17978 has been used extensively in studies of *A. baumannii* pathogenesis (30–32). To determine whether *A. baumannii* 17978 VU and 17978 UN variants exhibit differential fitness *in vivo*, both variants were assessed in a murine model of pneumonia, and bacterial burdens in the lungs and spleens of infected mice were compared at 24 and 36 h postinfection (h.p.i.). Mice

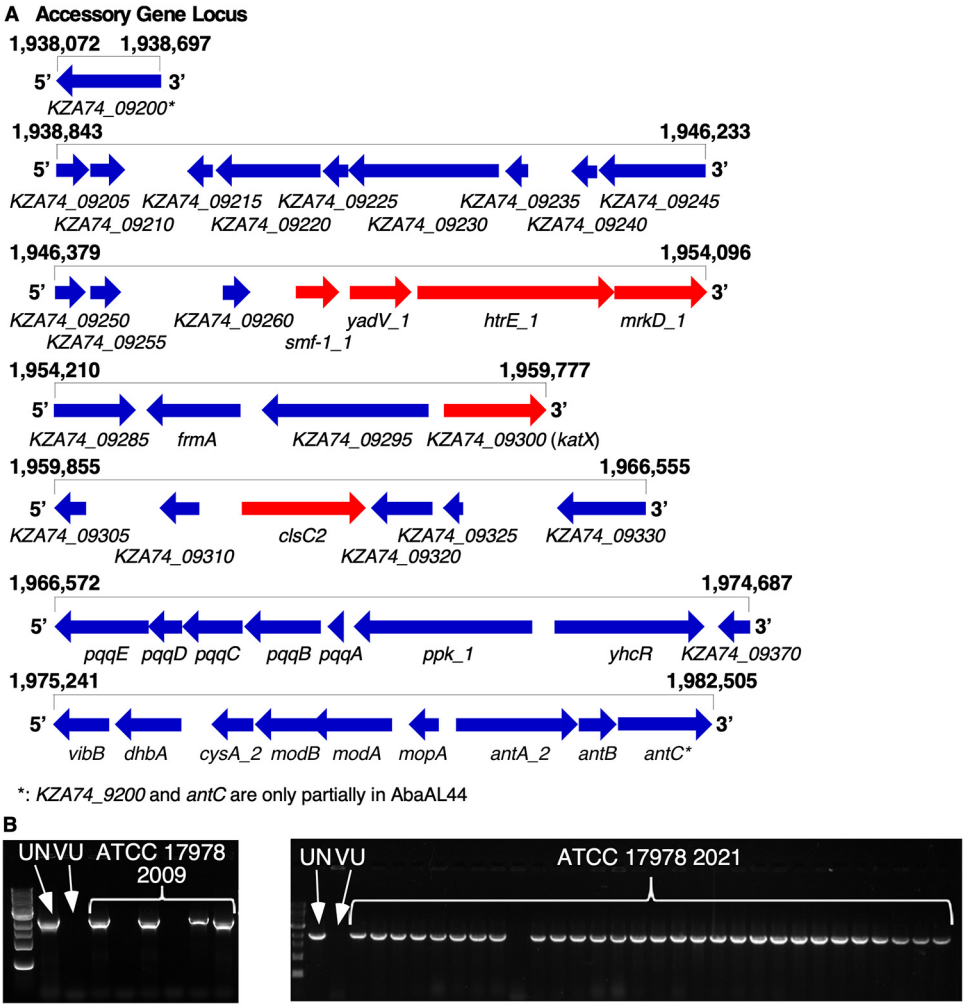

FIG 1 PacBio sequencing reveals structural differences between the genomes of *Acinetobacter baumanii* 17978 VU and 17978 UN variants. The genome sequences of *A. baumanii* 17978 VU and 17978 UN variants were determined by PacBio and Nanopore sequencing and subsequently compared to the genome of the reference strain, *A. baumannii* ATCC 17978-mff (RefSeq accession number NZ_CP012004.1). (A) Visual representation of AbaAL44, encompassing multiple accessory genes present in the genome of *A. baumannii* 17978 UN, based on analysis and inspection of a new *A. baumannii* 17978 UN reference genome (NCBI accession number CP079931). The relative position (in terms of base pair number) within the assembled genome of *A. baumannii* 17978 UN is indicated above each row, and gene names are indicated below each gene. Locus tags refer to CP079931. Arrows indicate the relative transcriptional direction of each gene. Genes indicated in red represent putative pathogenesis genes. (B) Images of agarose gel electrophoresis indicating the differential presence of the accessory *clsC2* gene within individual colonies of *A. baumannii* 17978 laboratory stocks based on PCR detection of *clsC2*. The VUMC laboratory stock (left) was obtained from ATCC in 2009, and the UIC laboratory stock (right) was obtained from ATCC in 2021. Presence of accessory *clsC2* indicates that an isolate belongs to *A. baumannii* 17978 UN variant.

infected with *A. baumannii* 17978 UN had a statistically significant decrease in lung bacterial burdens at both 24 and 36 h.p.i. compared to those of mice infected with *A. baumannii* 17978 VU (Fig. 2A and B). At 24 h.p.i., mice infected with *A. baumannii* 17978 UN had lost significantly more weight (Fig. 2C), suggesting an increase in morbidity relative to that of mice infected with *A. baumannii* 17978 VU. Histological examination of lungs from mice infected with *A. baumannii* 17978 UN revealed fewer visible bacteria within the alveolar spaces, and mice infected with *A. baumannii* 17978 UN exhibited reduced extrapulmonary dissemination to the spleen relative to that in mice infected with *A. baumannii* 17978 VU (Fig. 2D and E). Combined, these data suggest that *A. baumannii* 17978 UN exhibits decreased fitness in a murine model of pneumonia compared to that of *A. baumannii* 17978 VU.

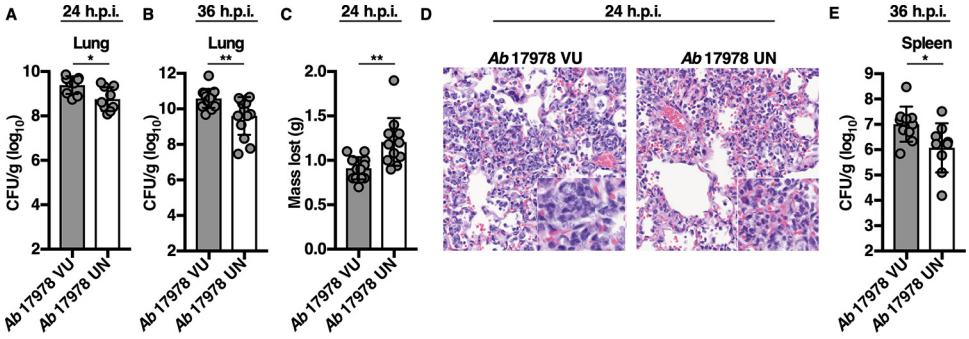

FIG 2 *A. baumannii* 17978 VU and 17978 UN variants exhibit differential virulence in a mouse model of pneumonia. Mice were challenged intranasally with 3×10^8 CFU of mid-log-phase *A. baumannii* 17978 VU or 17978 UN variants. At 24 (A and C) or 36 (B and E) h.p.i., mice were euthanized, and organs were harvested. (A and B) Bacterial burdens in the lungs of mice at 24 and 36 h.p.i., respectively. (C) Mean number of grams of total body weight lost by infected mice at 24 h.p.i. (D) Representative hematoxylin and eosin-stained lung sections of mice infected with *A. baumannii* 17978 VU (left) or *A. baumannii* 17978 UN (right) at 24 h.p.i. (E) Bacterial burdens in the spleens of mice at 36 h.p.i. (A, B, C, and E) Circles represent individual animals, columns depict the mean, and error bars show standard deviation of the mean. Means were compared using an unpaired Welch's *t* test. CFU/g, CFU per gram of organ homogenate. *, $P < 0.05$; **, $P < 0.01$. H&E, hematoxylin and eosin.

Mice infected with *A. baumannii* 17978 UN lost more weight than mice infected with *A. baumannii* 17978 VU (Fig. 2C), which could indicate inappetence or increased metabolic demand due to increased inflammation. Neutrophilic inflammation is a characteristic response to *A. baumannii* infection and is essential for host resistance to infection (46–48). To determine if *A. baumannii* 17978 VU and 17978 UN variants induce differential neutrophil recruitment, mice were challenged with either variant, and the relative abundances of immune cell populations in both the lungs and blood were determined. Relative to mice infected with *A. baumannii* 17978 VU, mice infected with *A. baumannii* 17978 UN exhibited a decrease in the abundance of T cells, B cells, and overall lymphocytes, and a statistically significant increase in the relative abundance of neutrophils in the lungs (Fig. 3A to D). However, no significant differences in the number or percentage of neutrophils or lymphocytes were detected in the blood of mice infected with *A. baumannii* 17978 VU relative to those in mice infected with *A. baumannii* 17978 UN (Fig. S2). These data demonstrate that *A. baumannii* 17978 UN promotes a shift toward neutrophilic inflammation upon pneumonic infection of mice relative to that in *A. baumannii* 17978 VU.

Neutrophil recruitment to the site of infection is dependent upon the production of cytokines and chemokines. Interleukin 1 beta (IL-1β) is a potent proinflammatory cytokine that promotes neutrophil recruitment and stimulates neutrophil survival (49–52), whereas IL-10 is an anti-inflammatory cytokine that impedes neutrophil recruitment to the site of infection (53, 54). To test the hypothesis that infection with *A. baumannii* 17978 UN potentiates neutrophilic lung inflammation by inducing differential cytokine or chemokine production by host cells, murine bone marrow-derived macrophages (BMDMs) were infected with *A. baumannii* 17978 VU or 17978 UN variants, and cytokines and chemokines were quantified from cell culture supernatants. BMDMs infected with *A. baumannii* 17978 UN produced significantly more IL-1β and less IL-10 compared to that produced by BMDMs infected with *A. baumannii* 17978 VU (Fig. 3E and F). In contrast, the production of the murine neutrophil chemokines KC and MIP-2 did not differ between BMDMs infected with *A. baumannii* 17978 UN and 17978 VU variants (Fig. 3G and H). No differences in serum or lung IL-1β levels were detected at 24 h.p.i. between mice infected with *A. baumannii* 17978 VU and 17978 UN variants (Fig. S3). These data demonstrate that host responses to two common variants of *A. baumannii* 17978 differ in terms of induced cytokine production by macrophages, as well as in the degree of induced neutrophilic lung inflammation, bacterial persistence in the lung, and dissemination to the spleen in a mouse model of pneumonia.

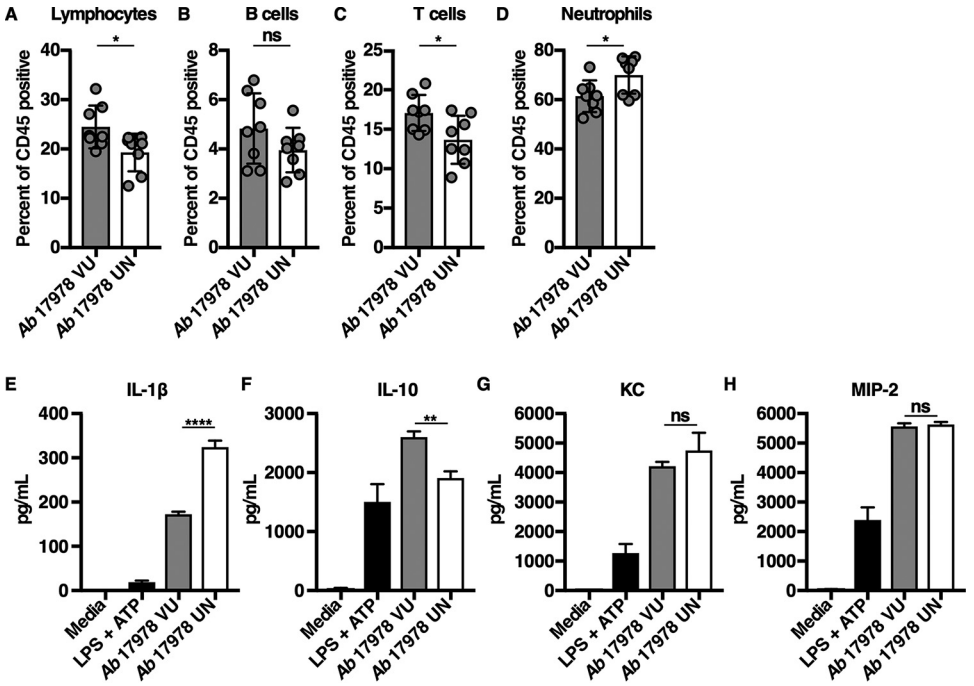

FIG 3 Mice infected with *A. baumannii* 17978 UN exhibit increased neutrophilic inflammation in comparison to that of mice infected with *A. baumannii* 17978 VU. (A to D) Mice were challenged intranasally with 3×10^8 CFU of mid-log-phase *A. baumannii* 17978 VU or 17978 UN. At 24 h.p.i., mice were euthanized, lungs were harvested, and immune cell recruitment to the lungs was quantified using flow cytometry analysis. (E to H) Murine bone marrow-derived macrophages (BMDMs) were infected with mid-log-phase cultures of *A. baumannii* 17978 VU or 17978 UN at a multiplicity of infection (MOI) of 10 and incubated at 37°C. At 18 h.p.i., supernatants of infected BMDMs were collected, and the concentrations of IL-1β (E), interleukin 10 (IL-10) (F), KC (G), or MIP-2 (H) in the supernatants of infected BMDMs were determined by enzyme-limited immunosorbent assay (ELISA). (A to D) Circles represent individual animals, columns depict the mean, and error bars show standard deviation of the mean. Means were compared using an unpaired Welch's *t* test. (E to H) $N = 3$ or 4 biological replicates per group per experiment. Experiments were repeated for a total of at least two times, with graphs depicting representative data. (E to H) Columns depict the mean, and error bars show standard deviation of the mean. Means were compared to the mean of the *A. baumannii* 17978 VU column using a one-way analysis of variance (ANOVA) adjusted for multiple comparisons. *, $P < 0.05$; **, $P < 0.01$; ****, $P < 0.0001$; ns, not significant.

The AbaAL44 *katX* gene promotes bacterial resistance to hydrogen peroxide stress and neutrophil-mediated killing. To interrogate the role of putative pathogenesis genes contained within AbaAL44 in the differential pathogenicity of *A. baumannii* 17978 UN, the candidate accessory pilus assembly locus comprising *smf-1*, *yadV*, *htrE*, and *mrkD*; the accessory catalase gene (*KZA74_09300*; *katX*); or the accessory cardiolipin synthase gene (*clsC2*) was replaced with a kanamycin resistance cassette to create *A. baumannii* 17978 UN Δ*smf-1_1-mrkD_1*::*kan* (*A. baumannii* 17978 UN Δ*pilus*), 17978 UN Δ*KZA74_09300*::*kan* (17978 UN Δ*katX*), and 17978 UN Δ*clsC2*::*kan* (17978 UN Δ*clsC2*) strains, respectively (55). Type I pili are bacterial surface appendages involved in bacterial uptake by macrophages, biofilm formation, attachment to host cells, motility, and agglutination of red blood cells (56–59). However, the *A. baumannii* 17978 UN Δ*pilus* strain did not differ from *A. baumannii* 17978 UN in terms of bacterial uptake by macrophage-like RAW 264.7 cells (Fig. S4A), biofilm formation (Fig. S4B), bacterial attachment to A549 epithelial cells (Fig. S4C), bacterial surface-associated motility (Fig. S4D), hemagglutination of human erythrocytes (Fig. S4E), or differential production of cytokines by infected BMDMs (Fig. S4F and G). These data suggest that the type I pilus locus does not contribute to the interactions with host cells under these *in vitro* conditions.

Catalases are enzymes that catalyze the decomposition of hydrogen peroxide (H_2O_2) to water and oxygen and thereby protect bacteria from reactive oxygen species (ROS)-mediated oxidative stress and killing by innate immune cells (60–62). To test the

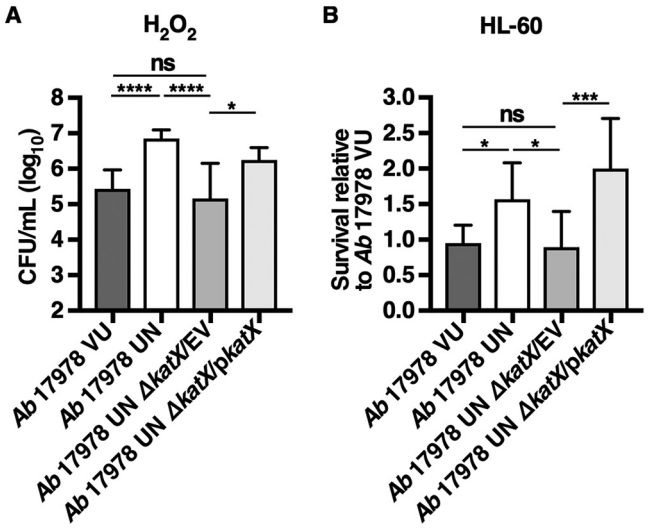

FIG 4 The AbaAL44 *katX* gene promotes bacterial resistance to hydrogen peroxide stress and neutrophil-mediated killing. (A) Mid-log-phase *A. baumannii* 17978 VU, 17978 UN, 17978 UN Δ*katX*/EV, or 17978 UN Δ*katX*/p*katX* variants were incubated in LB medium supplemented with 1 mM hydrogen peroxide at a starting inoculum of 1×10^7 CFU/ml. Following a 30-min incubation, remaining viable bacteria were enumerated. (B) Differentiated neutrophil-like HL-60 cells were incubated with mid-log-phase *A. baumannii* 17978 VU, 17978 UN, 17978 UN Δ*katX*/EV, or 17978 UN Δ*katX*/p*katX* variants at an MOI of 2. At 90 min postincubation, HL-60 cells were lysed, and neutrophil-mediated killing of bacteria was assessed by determining the number of viable bacteria in each well. Data are represented as bacterial survival relative to that for *A. baumannii* 17978 VU. In both panels, $N = 3$ or 4 biological replicates per group per experiment. Experiments were repeated for a total of at least two times, with graphs depicting average data. Columns depict the mean, and error bars show standard deviation of the mean. All means were compared to all other means using a one-way ANOVA adjusted for multiple comparisons. *, $P < 0.05$; ***, $P < 0.001$; ****, $P < 0.0001$; ns, not significant.

hypothesis that the AbaAL44 accessory catalase present in *A. baumannii* 17978 UN contributes to bacterial resistance to oxidative stress, the relative susceptibilities of *A. baumannii* 17978 VU, 17978 UN, 17978 UN Δ*katX*/empty vector (EV), and 17978 UN Δ*katX* in which the AbaAL44 *katX* gene was expressed in *trans* (*A. baumannii* 17978 UN Δ*katX*/p*katX*) to hydrogen peroxide stress *in vitro* was determined. Thirty minutes after incubation of 1×10^7 CFU/ml of bacteria in the presence of 1 mM hydrogen peroxide, the density of viable *A. baumannii* 17978 UN bacteria remained virtually unchanged at approximately 7 log_{10} CFU/ml. In contrast, the densities of viable *A. baumannii* 17978 VU and 17978 UN Δ*katX*/EV bacteria were significantly reduced to approximately 5.5 log_{10} CFU/ml. Expression of the AbaAL44 *katX* in *trans* restored hydrogen peroxide stress resistance in the *A. baumannii* 17978 UN Δ*katX*/p*katX* strain to levels approximating those in the parental strain (Fig. 4A). These data indicate that the *katX* present in AbaAL44 enhances bacterial resistance to oxidative stress *in vitro*. Neutrophils are innate immune effector cells that phagocytose and subsequently kill engulfed pathogens using an array of antimicrobial molecules, including ROS produced by the enzyme NADP (NADPH) oxidase (63, 64). Based on this, we hypothesized that the *katX* present in *A. baumannii* 17978 UN promotes bacterial resistance to neutrophil-mediated killing. To test this, differentiated neutrophil-like HL-60 cells were incubated with *A. baumannii* 17978 UN, 17978 VU, 17978 UN Δ*katX*/EV, or 17978 UN Δ*katX*/p*katX* strains and bacterial resistance to neutrophil-mediated extracellular and intracellular killing was determined by measuring relative bacterial survival postincubation. After incubation in the presence of differentiated neutrophil-like HL-60 cells, relative survival of *A. baumannii* 17978 UN was significantly greater than that of both the 17978 VU and 17978 UN Δ*katX*/EV strains (Fig. 4B). Similar results were obtained with murine bone marrow-derived neutrophils (Fig. S5). In *trans* expression of AbaAL44 *katX*

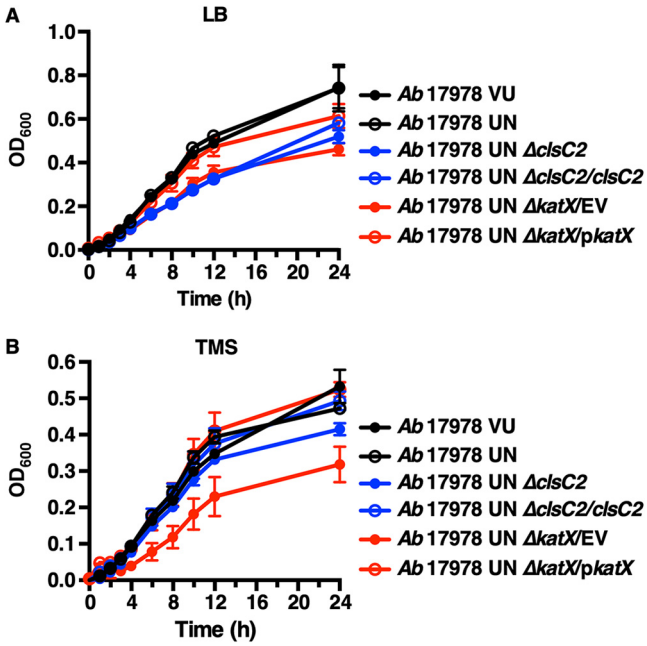

FIG 5 AbaAL44 *clsC2* and *katX* mutants generated in the *A. baumannii* 17978 UN background exhibit growth defects *in vitro*. (A and B) Stationary-phase cultures of the indicated strains of *A. baumannii* were normalized to a similar optical density at 600 nm (OD_{600}) and inoculated into fresh rich medium (LB) or minimal medium (Tris minimal succinate [TMS]). Growth was assayed by measuring OD_{600} over time. Symbols depict the mean, and error bars show standard deviation of the mean. $N = 3$ or 4 biological replicates per group per experiment. Graphs depict representative data from two independent experiments. For 8-, 10-, and 12-h time points, the means of *A. baumannii* 17978 UN Δ*clsC2*, 17978 UN Δ*clsC2*/*clsC2*, 17978 UN Δ*katX*/EV, 17978 UN Δ*katX*/p*katX*, and 17978 UN variants were compared using a one-way ANOVA adjusted for multiple comparisons. (A) Differences between *A. baumannii* 17978 UN and 17978 UN Δ*clsC2*, 17978 UN Δ*clsC2*/*clsC2*, or 17978 UN Δ*katX*/EV variants: $P < 0.0001$ for each comparison for each time point. Difference between *A. baumannii* 17978 UN and 17978 UN Δ*katX*/p*katX* variants: $P < 0.05$ for the10-h time point and $P > 0.05$ for 8- and 12-h time points. (B) Differences between *A. baumannii* 17978 UN and 17978 UN Δ*clsC2*, 17978 UN Δ*clsC2*/*clsC2*, or 17978 UN Δ*katX*/p*katX* variants: $P > 0.05$ for each comparison for each time point. Difference between *A. baumannii* 17978 UN and 17978 UN Δ*katX*/EV variants: $P < 0.0001$, $P < 0.0001$, or $P < 0.001$ for 8-, 10-, and 12-h time points, respectively.

restored survival of the *A. baumannii* 17978 UN Δ*katX*/EV strain to the levels of the parental strain (Fig. 4B). Deletion of the AbaAL44 *katX* gene negatively affected the growth of *A. baumannii* 17978 UN *in vitro* in both rich (lysogeny broth [LB]) and minimal (Tris minimal succinate [TMS]) media, which was restored by expressing AbaAL44 *katX* in *trans* (Fig. 5). Taken together, these data suggest that the *katX* present in AbaAL44 contributes to *A. baumannii* 17978 UN growth *in vitro*, as well as to bacterial resistance to oxidative stress and neutrophil-mediated killing.

AbaAL44 *clsC2* contributes to bacterial resistance to cell envelope stress and affects bacterial interactions with host immune cells. Bacterial cardiolipin synthases are enzymes that utilize phosphatidylglycerol (PG) and/or phosphatidylethanolamine (PE) as substrates to catalyze the formation of cardiolipin (65, 66). Cardiolipin is one of several anionic phospholipids that comprise the Gram-negative cell envelope, and, in *Escherichia coli*, it has been demonstrated to localize to the cellular poles (67). Because cardiolipin promotes bacterial resistance to envelope stressors such as high salinity (68, 69), it was hypothesized that *A. baumannii* 17978 UN is more resistant to conditions of high salinity than the *A. baumannii* 17978 UN Δ*clsC2* strain. To test this, the susceptibility to conditions of high salinity of *A. baumannii* 17978 VU, 17978 UN, 17978 UN Δ*clsC2*, and 17978 UN Δ*clsC2* in which *clsC2* has been reintroduced chromosomally under its native promoter by mini-Tn*7* integration (*A. baumannii* 17978 UN Δ*clsC2*/*clsC2*) was determined by comparing bacterial survival after incubation in LB supplemented with 2.5 M NaCl. After 2 h of incubation in high salinity, bacterial survival of

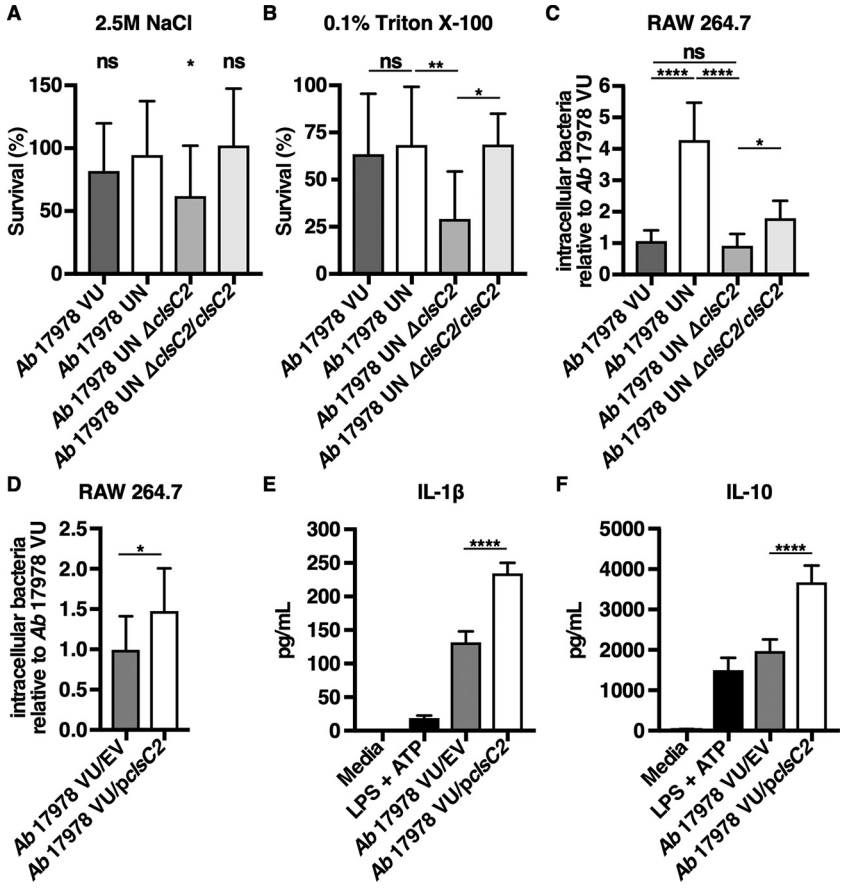

FIG 6 The AbaAL44 *clsC2* gene contributes to bacterial resistance to cell envelope stress and affects bacterial interactions with host immune cells. (A) Mid-log-phase *A. baumannii* 17978 VU, 17978 UN, 17978 UN Δ*clsC2*, or 17978 UN Δ*clsC2*/*clsC2* variants were inoculated into LB medium supplemented with 2.5 M NaCl at a starting inoculum of 1×10^7 CFU/ml, and incubated at 37°C for 2 h. After 2 h of incubation, bacterial viability was determined for each strain, and bacterial survival was calculated as the percentage of viable bacteria postincubation relative to the number of viable bacteria preincubation. (B) Mid-log-phase *A. baumannii* 17978 VU, 17978 UN, 17978 UN Δ*clsC2*, or 17978 UN Δ*clsC2*/*clsC2* variants were inoculated into phosphate-buffered saline (PBS) supplemented with 0.1% Triton X-100 at a starting inoculum of 1×10^{10} CFU/ml and incubated at 37°C for 6 h. After incubation, bacterial viability was determined for each strain, and survival was calculated as described above. (C and D) Macrophage-like RAW 264.7 cells were infected with mid-log-phase *A. baumannii* 17978 VU, 17978 UN, 17978 UN Δ*clsC2*, 17978 UN Δ*clsC2*/*clsC2*, 17978 VU/EV, or 17978 VU/p*clsC2* at an MOI of 15, and extracellular bacteria were killed with gentamicin at 30 min postinfection. Thirty minutes after the addition of gentamicin, RAW cells were washed and lysed, and intracellular bacterial burdens were determined. (E and F) Murine bone marrow-derived macrophages were infected with mid-log-phase cultures of *A. baumannii* 17978 VU/EV or *A. baumannii* 17978 VU/p*clsC2* at an MOI of 10 and incubated at 37°C. At 18 h.p.i., supernatants of infected BMDMs were collected, and the concentrations of IL-1β (E) or IL-10 (F) in the supernatants of infected BMDMs were determined by ELISA. (A to D) $N = 3$ or 4 biological replicates per group per experiment. Graphs depict average results from at least three independent experiments. (E and F) $N = 4$ biological replicates per group per experiment. Graphs depict representative data. In all panels, columns depict the mean, and error bars show standard deviation of the mean. Means were compared to the mean of *A. baumannii* 17978 UN (A) or to all other means (B to F) using Welch's *t* test (D) or one-way ANOVA adjusted for multiple comparisons (A, B, C, E and F). *, $P < 0.05$; **, $P < 0.01$; ****, $P < 0.0001$; ns, not significant.

the *A. baumannii* 17978 UN Δ*clsC2* strain was significantly reduced by approximately 30% compared to the survival of 17978 UN. After incubation in high salinity, survival of the *A. baumannii* 17978 UN Δ*clsC2/clsC2* strain did not differ significantly from that of 17978 UN (Fig. 6A). Perturbations in bacterial membrane phospholipid homeostasis involving cardiolipin have been demonstrated to increase bacterial susceptibility to molecular detergents such as surfactants, which are found in high concentrations in

the lungs and may be relevant to bacterial pneumonia pathogenesis (70). To determine if the AbaAL44 *clsC2* present in *A. baumannii* 17978 UN promotes bacterial resistance to detergents, the susceptibility of *A. baumannii* 17978 VU, 17978 UN, 17978 UN Δ*clsC2*, and 17978 UN Δ*clsC2/clsC2* variants to the detergent Triton X-100 was assessed. After 6 h of incubation in 0.1% Triton X-100, bacterial survival of *A. baumannii* 17978 UN Δ*clsC2* was significantly less than that of 17978 UN. Survival of *A. baumannii* 17978 UN Δ*clsC2/clsC2* was significantly greater than that of 17978 UN Δ*clsC2*, and similar to that of 17978 UN (Fig. 6B). Taken together, these data indicate that the accessory cardiolipin synthase gene present in *A. baumannii* 17978 UN contributes to this strain's resistance to conditions of high salinity and detergent stress.

Previous work has demonstrated that cardiolipin promotes uptake of bacteria by professional phagocytes such as macrophages through the scavenger receptor CD36 (71). Therefore, it was hypothesized that the previously observed increase in intracellular bacterial burden in macrophage-like RAW cells infected with *A. baumannii* 17978 UN is mediated by the AbaAL44 *clsC2* (Fig. S4A). To test this, the relative intracellular bacterial burdens of RAW cells infected with *A. baumannii* 17978 VU, 17978 UN, 17978 UN Δ*clsC2*, or 17978 UN Δ*clsC2*/*clsC2* variants were determined. The intracellular bacterial burden of RAW cells infected with the *A. baumannii* 17978 UN Δ*clsC2* variant was significantly reduced by approximately 75% relative to the intracellular bacterial burden of RAW cells infected with *A. baumannii* 17978 UN and was similar to the intracellular bacterial burden of RAW cells infected with 17978 VU. There was a small but statistically significant increase in the intracellular bacterial burden of RAW cells infected with the *A. baumannii* 17978 UN Δ*clsC2*/*clsC2* variant relative to that of RAW cells infected with the 17978 UN Δ*clsC2* variant (Fig. 6C). Expression of *clsC2* in *trans* in *A. baumannii* 17978 VU (*A. baumannii* 17978 VU/p*clsC2*) also significantly increased the intracellular bacterial burden of infected RAW cells compared to that of RAW cells infected with *A. baumannii* 17978 VU/EV (Fig. 6D). These data suggest that the AbaAL44 *clsC2* gene contributes to *A. baumannii* 17978 UN phagocytosis by macrophages.

Chromosomal reintroduction of *clsC2* in the *A. baumannii* 17978 UN Δ*clsC2* variant did not fully restore phagocytosis by infected RAW cells to the levels observed with *A. baumannii* 17978 UN (Fig. 6C). The deletion of *clsC2* negatively affected the growth of *A. baumannii* 17978 UN *in vitro* in rich medium (LB), but not in minimal medium (TMS) (Fig. 5). The growth defect of *A. baumannii* 17978 UN Δ*clsC2* in rich medium was also not restored by chromosomal reintegration of *clsC2* under its native promoter (Fig. 5A). Furthermore, the supernatants of RAW cells infected with the *A. baumannii* 17978 UN Δ*clsC2* or 17978 UN Δ*clsC2*/*clsC2* variants contained small, punctate colonies (Fig. S6B). These colonies were also present in lysates of RAW cells infected with *A. baumannii* 17978 UN Δ*clsC2* or 17978 UN Δ*clsC2*/*clsC2* variants that were collected prior to treatment with gentamicin, but were absent from the starting inoculums (Fig. S6A and C). Small, punctate colonies were not observed in any samples collected from RAW cells infected with the *A. baumannii* 17978 UN parental strain (Fig. S6). These findings suggest a reduction in the fitness of the *A. baumannii* 17978 UN Δ*clsC2* strain that is not restored by integration of *clsC2* elsewhere on the chromosome and are indicative of another genetic difference between the parental *A. baumannii* 17978 UN and the Δ*clsC2* derivative or polar effects of the inserted kanamycin cassette. As expression of *clsC2* in *A. baumannii* 17978 VU resulted in an increase in macrophage phagocytosis, the differential growth phenotype between the 17978 UN and 17978 UN Δ*clsC2* variants was not pursued further.

Mitochondrial cardiolipin activates the NLRP3 inflammasome, resulting in the production of IL-1β, and saturated cardiolipins increase IL-1β production through Toll-like receptor 4 (TLR4) signaling (72, 73). This raised the hypothesis that the increase in IL-1β production observed in macrophages infected with *A. baumannii* 17978 UN is due to the presence of AbaAL44 *clsC2*. Given the reduced fitness of the Δ*clsC2* mutant in the *A. baumannii* 17978 UN background, this hypothesis was tested by expressing the AbaAL44 *clsC2* gene in *trans* in 17978 VU, which naturally lacks AbaAL44 and thus

clsC2. BMDMs were infected with *A. baumannii* 17978 VU/EV or 17978/p*clsC2,* and the concentrations of proinflammatory IL-1β and anti-inflammatory IL-10 in the supernatants of infected BMDMs were determined at 18 h.p.i. Relative to infection with *A. baumannii* 17978 VU/EV, infection with 17978 VU/p*clsC2* significantly increased the production of IL-1β by infected BMDMs (Fig. 6E). These findings indicate that the presence of AbaAL44 *clsC2* increases proinflammatory IL-1β production by macrophages infected with *A. baumannii* 17978 UN. Infection with *A. baumannii* 17978 UN decreases the production of IL-10 by infected macrophages relative to that after infection with 17978 VU (Fig. 3F). In contrast, expression of *clsC2* in *A. baumannii* 17978 VU significantly increased IL-10 production by infected macrophages (Fig. 6F). This finding suggests that the decrease in IL-10 production observed in macrophages infected with *A. baumannii* 17978 UN cannot be explained by the presence of *clsC2* alone. Together, these data indicate that AbaAL44 influences the interactions between *A. baumannii* and the host.

DISCUSSION

The process by which *A. baumannii* acquires or loses resistance to antimicrobials from gain or loss of genetic material is well characterized (21, 35). In contrast, less is known about how such genomic plasticity affects *A. baumannii* pathogenicity. Here, the discovery that two variants of *A. baumannii* ATCC 17978 differ based on the presence of the AbaAL44 accessory locus encompassing several pathogenesis genes is described. Review of the 5,301 publicly available *A. baumannii* genome assemblies in the NCBI database revealed that genetic elements similar to AbaAL44 are present in at least 100 strains of *A. baumannii*. Of the 8 *A. baumannii* ATCC 17978 genome sequences published in NCBI, AbaAL44 is not present in any of them, but AbaAL44 is present in the *A. baumannii* 17978 genome sequence published by the ATCC in 2019 (https://genomes.atcc.org/genomes/e1d18ea4273549a0). However, if laboratories assemble sequenced genomes of their *A. baumannii* 17978 laboratory stocks to a reference genome that does not include AbaAL44 (e.g., NCBI accession number NZ_CP018664), the presence of AbaAL44 in these sequenced genomes would not be detected. When combined with the data presented here, these findings suggest that the differential presence of AbaAL44 is a common structural genetic variant among *A. baumannii* strains and that laboratories studying *A. baumannii* ATCC 17978 may be working with either variant without awareness or may be working with cultures containing a mix of the two variants. The differential presence of AbaAL44 among two variants of a type strain is most likely due to loss of AbaAL44 by *A. baumannii* 17978 VU during the course of laboratory propagation. Adaptive loss of genetic material has been previously described for *Acinetobacter* spp. (74). Furthermore, genetic differences among lineages of a given laboratory strain have previously been demonstrated for other species. Continuous maintenance and propagation of *Pseudomonas aeruginosa* strain PAO1 in laboratories throughout the world has led to substantial genotypic differences among sublines of this strain (75), and two lineages of *Clostridioides difficile* R20291 differ based on a small number of single-nucleotide genomic changes, which lead to distinct phenotypic differences (76).

A. baumannii 17978 VU and 17978 UN variants exhibit differential fitness in a mouse model of pneumonia, which is likely due in part to the differential presence of AbaAL44. Putative pathogenesis genes present in AbaAL44, including the *katX* and *clsC2* genes, increase *A. baumannii* 17978 UN resistance to oxidative stress, neutrophil-mediated killing, and surfactant stress. *A. baumannii* encounters hydrogen peroxide, the substrate of catalase enzymes, and surfactant inside the mouse lung (77, 78), and neutrophils are an essential component of the host immune response to infection with this pathogen (46–48). As such, the presence of accessory *katX* and *clsC2* genes may confer some *in vivo* advantage to *A. baumannii* 17978 UN. *A. baumannii* 17978 UN also potentiates neutrophilic lung inflammation *in vivo* and increases the production of proinflammatory IL-1β by infected macrophages. This increase in inflammation and

neutrophil recruitment to the site of infection may overwhelm any increased bacterial resistance to neutrophil-mediated killing in *A. baumannii* 17978 UN, resulting in net decreased bacterial survival inside the mouse lung. The effects of other genes contained in AbaAL44 or polymorphisms elsewhere on the chromosome on *A. baumannii* fitness have not been interrogated but may contribute to the net differences in pathogenesis between these variants.

As IL-1β promotes the recruitment of neutrophils to the site of infection (49), the increased production of proinflammatory IL-1β by macrophages infected with *A. baumannii* 17978 UN is likely to play a role in the shift toward neutrophilic inflammation observed in infected mice. Although differences in IL-1β concentration at 24 h.p.i. between mice infected with *A. baumannii* 17978 VU and mice infected with *A. baumannii* 17978 UN were not observed, such differences may occur earlier in the course of infection, culminating in the differential abundance of neutrophils observed at 24 h.p.i. Mitochondrial cardiolipin is a known activator of the NLRP3 inflammasome resulting in the production of IL-1β, and saturated cardiolipins increase IL-1β production in a TLR4-dependent manner (72, 73). In *trans* expression of *clsC2* in *A. baumannii* 17978 VU increased IL-1β production by infected macrophages, suggesting that the presence of the AbaAL44 *clsC2* gene in *A. baumannii* 17978 UN may increase cell envelope cardiolipin content, resulting in NLRP3 inflammasome activation and enhanced IL-1β production by macrophages.

Infection with *A. baumannii* 17978 UN resulted in decreased IL-10 production by infected macrophages relative to that produced during infection with *A. baumannii* 17978 VU. Mitochondrial cardiolipin inhibits IL-10 production by recruiting a repressor complex to the *IL-10* promoter. The reduction in anti-inflammatory IL-10 promotes persistent inflammation in experimental bacterial pneumonia (79, 80). It is conceivable that bacterial cardiolipin similarly inhibits IL-10 production and that modulation of bacterial cardiolipin content through the AbaAL44 *clsC2* gene is responsible for modulating macrophage IL-10 production. However, macrophage infection with a strain of *A. baumannii* 17978 VU in which *clsC2* was expressed in *trans* did not recapitulate this finding. Paradoxically, macrophage infection with *A. baumannii* 17978 VU/p*clsC2* increased IL-10 production. This suggests that the presence of *clsC2* alone cannot explain the relative decrease in IL-10 production observed in macrophages infected with *A. baumannii* 17978 UN. Regulation of IL-10 production by immune cells is complex, and multiple factors affect its expression (81). Bacterial products such as cell wall components and lipopolysaccharide (LPS) increase macrophage IL-10 production through TLR2- and TLR4-mediated signaling, respectively (81, 82). In contrast, interferon gamma (IFN-γ) inhibits IL-10 production (81). IFN-γ production by macrophages is induced by IL-18, which, like IL-1β, is a product of NLRP3 inflammasome activation, and IL-1β production is increased in macrophages infected with *A. baumannii* 17978 UN (83–85). Therefore, any combination of these factors may account for the differences in IL-10 production between macrophages infected with *A. baumannii* 17978 UN and macrophages infected with 17978 VU/p*clsC2*. Other genes contained in AbaAL44 or other genetic differences between the two *A. baumannii* 17978 variants may also account for the differential cytokine production by macrophages infected with 17978 UN.

This study demonstrates that the AbaAL44 *katX* and *clsC2* genes are advantageous to *A. baumannii* 17978 UN survival *in vitro*. Specifically, the AbaAL44 *katX* gene present in *A. baumannii* 17978 UN increases bacterial resistance to oxidative stress. In addition to the AbaAL44 *katX* gene described in this study, two catalase genes—*katE* and *katG*—have previously been identified in *A. baumannii* (86). Increased transcription of *katG* as a consequence of upstream insertion of IS*Aba1* has been demonstrated to increase *A. baumannii* resistance to oxidative stress (87). Taken together, these findings highlight the importance of catalases in *A. baumannii* pathogenesis and provide an example of how increasing bacterial catalase gene abundance can contribute to *A. baumannii* pathogenicity.

The findings presented here implicate a dichotomous role for the AbaAL44 *clsC2* gene in *A. baumannii* 17978 UN. While this gene promotes the uptake of *A. baumannii*

17978 UN by phagocytes, its presence also increases 17978 UN resistance to envelope stressors, such as surfactants. These findings are consistent with previous reports demonstrating that membranes with bacterial cardiolipin on their surfaces promote macrophage phagocytosis through the scavenger receptor CD36 (71) and that bacterial cardiolipin promotes resistance to osmotic and surfactant stress (69, 70). Cardiolipin has also been demonstrated to increase *A. baumannii* resistance to cationic antimicrobial peptides, another type of envelope stressor, suggesting that increasing cell envelope cardiolipin content is a relevant survival strategy for this pathogen (88). In addition to the accessory *clsC2* described in this study, both *A. baumannii* 17978 VU and 17978 UN variants contain two additional cardiolipin synthase genes. To our knowledge, however, the role of these genes in *A. baumannii* biology and pathogenesis remains to be fully elucidated. It has previously been reported that *A. baumannii* cell membranes contain a variety of unique, coexisting cardiolipin species (89). In *E. coli*, different cardiolipin synthase genes are active during distinct stages of bacterial growth (66). It is possible that the three cardiolipin synthase genes present in *A. baumannii* may be expressed during different growth phases and/or may be responsible for synthesizing distinct species of cardiolipin. This notion is supported by recent findings demonstrating that individual enzymes of the same family are implicated in the production of either cardiolipin or monolysocardiolipin, an intermediate species in the cardiolipin remodeling pathway, in *A. baumannii* (88, 90). The *in vitro* growth defect and reduced uptake by RAW cells observed in the *A. baumannii* 17978 UN Δ*clsC2* variant could not be restored to the levels of the parental strain by chromosomally reintroducing *clsC2* under its native promoter. This may be due to unidentified genetic differences between the Δ*clsC2* mutant and the parental *A. baumannii* 17978 UN strain, or due to polar effects of the Δ*clsC2*::*kan* deletion-insertion on nearby genes. However, expression of AbaAL44 *clsC2* in the Ab 17978 VU strain increased phagocytosis and IL-1β production by macrophages indicating that *clsC2* impacts *A. baumannii* interactions with the host.

Together, these findings indicate that two genotypically and phenotypically distinct variants of the common type strain, *A. baumannii* ATCC 17978, exist and are indiscriminately used in published studies of *A. baumannii* (91). As such, careful genotyping and phenotyping of *A. baumannii* type strains by individual laboratories may be warranted. Furthermore, this study demonstrates how *A. baumannii* genomic plasticity can affect pathogenicity and interactions with the host.

MATERIALS AND METHODS

Bacterial strains and culture conditions. Bacterial strains and plasmids used in this study are listed in Table S1 in the supplemental material. *A. baumannii* 17978 UN and 17978 VU variants were received from ATCC in 2009 and in March 2021. Strains were maintained as frozen stocks in lysogeny broth (LB) supplemented with 30% (vol/vol) glycerol at −80°C. Unless noted otherwise, bacteria were grown on LB agar (LBA) at 37°C, and single, isolated colonies were resuspended in LB and incubated overnight at 37°C with constant agitation. Overnight cultures were diluted 1:100 in fresh LB and incubated for 3.5 h at 37°C with constant agitation until the exponential phase. Exponential-phase cultures were washed twice with cold phosphate-buffered saline (PBS) and diluted to 1×10^{10} CFU/ml in PBS. Bacterial cultures were diluted further as appropriate for each experiment.

Genome sequencing and analyses. The genomes of *A. baumannii* strains 17978 VU and 17978 UN variants were sequenced using PacBio sequencing by Genewiz (South Plainfield, NJ) (45). Pangenomes were assembled and annotated as follows. The raw sequence reads of the strains of *A. baumannii* were assembled using Flye version 2.4.2 with the genome size set to 3.86 Mb, choosing the option for plasmid assembly and three polishing iterations. An Amazon Web Services (AWS) EC2 m5.2xlarge instance was used for all of the assembly runs. Assembly statistics were compared and analyzed using Quast version 5.0.2 against the reference *A. baumannii* ATCC 17978-mff genome from NCBI (RefSeq accession number NZ_CP012004.1). The assembled genomes were annotated using Prokka version 1.13.5. Pangenomes were created from these annotated genomes using Roary version 3.12.0 with the options "-e -n -v." Average nucleotide identity (ANI) of the genomes of *A. baumannii* 17978 VU and 17978 UN variants was determined using an online ANI calculator (http://enve-omics.ce.gatech.edu/ani/). The assembled genomes of *A. baumannii* 17978 VU and 17978 UN variants are available in the NCBI database (accession numbers CP079213 for *A. baumannii* 17978 VU and CP079212 for *A. baumannii* 17978 UN). Additionally, *A. baumannii* 17978 UN received from ATCC in 2021 was sequenced using Nanopore long-read sequencing technology by the Microbial Genome Sequencing Center (MiGS; Pittsburgh, PA). This reference genome sequence was deposited in NCBI and annotated using the Prokaryotic Genome Annotation

Pipeline (PGAP) (accession numbers as follows: chromosome, CP079931; pAB3, CP079932; pAB1, CP079933; pAB2, CP079934).

To screen for other differences between the genomes of *A. baumannii* 17978 VU and 17978 UN variants, such as SNPs, the genomes of both variants were sequenced as follows. DNA was isolated from *A. baumannii* 17978 UN and 17978 VU variants using a Wizard genomic DNA purification kit (Promega) or a DNeasy blood and tissue kit (Qiagen). DNA concentration was estimated with NanoDrop (Thermo). Library preparation by Nextera Flex and sequencing by Illumina NovaSeq 2 × 150-bp reads were performed at University of Illinois at Chicago Sequencing Core (UICSQC) or 2 × 100 bp reads at MiGS. The resulting reads were mapped to the ATCC *A. baumannii* 17978 VU genome (NCBI accession numbers NZ_CP012004, NZ_CP012005, CP000522.1, and CP000523.1) or to the *A. baumannii* 17978 UN genome (accession numbers CP079931, CP079932, CP079933, and CP079934) using breseq version 0.35.5 with default settings (92, 93).

To screen for the presence of AbaAL44 in Vanderbilt University Medical Center (VUMC) and University of Illinois Chicago (UIC) laboratory *A. baumannii* 17978 stocks, individual colonies were screened for the presence of the accessory *clsC2* gene by standard PCR using primers specific to this gene (forward primer, TCTTTCTGGCTGGTTGCTTACTCAGC; reverse primer, CCGCAGCTTTCTGATTGAGACAGGC). PCR products were visualized on an agarose gel. The presence of a PCR product indicated the presence of *clsC2*, signifying that that particular colony belonged to the *A. baumannii* 17978 UN variant. The absence of a PCR product indicated the absence of *clsC2*, signifying that that particular colony belonged to the *A. baumannii* 17978 VU variant.

Construction of *A. baumannii* 17978 UN Δ*pilus*, 17978 UN Δ*katX*, and 17978 UN Δ*clsC2* variants and complemented strains. *A. baumannii* 17978 UN Δ*pilus*, 17978 UN Δ*katX*, and 17978 UN Δ*clsC2* variants were constructed by recombineering using the protocol by Tucker et al. (55). Briefly, primers were designed that include approximately 125 bp of sequence upstream of the gene/locus to be deleted fused to the kanamycin resistance (*kan*^{r}) cassette forward primer, CCGGAATTGCCAGCTGGG, and 125 bp of sequence downstream of the gene/locus to be deleted fused to the *kan*^{r} cassette reverse primer, TTCAGAAGAACTCGTCAAG (Integrated DNA Technologies). These primer pairs were used to amplify the *kan*^{r} cassette from pCR2.1 plasmid DNA (Invitrogen). After purification, approximately 10 μg of each amplification product was electroporated into electrocompetent *A. baumannii* 17978 UN cells containing the recombinase plasmid pAT02. Transformants were recovered at 37°C with shaking in LB containing 2 mM isopropyl-β-D-thiogalactopyranoside (IPTG) for 4 h to induce recombinase expression prior to plating onto LB agar containing kanamycin. Kanamycin-resistant colonies were purified by serial passage and confirmed to have the appropriate deletion in the following two ways: first, by the difference in size of PCR amplification products using primers that amplify the recombineered locus by binding the chromosome outside the flanking sequences included in the recombineering primers, and second, by PCR amplification using a primer that binds within the *kan*^{r} cassette and a primer that binds the chromosome outside of the flanking sequence included in the recombineering primer.

For the *A. baumannii* 17978 UN Δ*katX* variant, the genetic defect was restored by expressing the accessory *katX* gene in *trans* as follows. *katX* was PCR amplified using a forward primer annealing to the region upstream of *katX* (GTAATTGGATGAGGTGATGTATTAG) and a reverse primer annealing to the region downstream of *katX* (GGCCATCCTCATCAAATACTG). Forward and reverse primers contained a 20-nucleotide sequence that overlapped the BamHI- or SalI-digested plasmid, respectively. Subsequently, the amplicon was ligated into the BamHI and SalI restriction sites of the *E. coli-A. baumannii* shuttle vector pWH1266 under its native promoter using NEBuilder HiFi DNA assembly (New England Biolabs, Ipswich, MA) to create pWH1266(*katX*) (77). Appropriate plasmid constructs were electroporated into the *A. baumannii* 17978 UN Δ*katX* variant as described above.

For the *A. baumannii* 17978 UN Δ*clsC2* variant the genetic defect was restored by reintegrating the accessory *clsC2* gene under its native promoter into a different part of the bacterial chromosome using methods described elsewhere (94). Briefly, *clsC2* was cloned into the pKNOCK-mTn*7* plasmid to make pKNOCK(*clsC2*) as described above, using a forward primer annealing to the region upstream of *clsC2* (CGCATCTTATAACGACAAAGAGAAC) and a reverse primer annealing to the region downstream of *clsC2* (GGGCGATAAAGCCACAGATAC). Next, the *E. coli λpir116* strain was transformed with pKNOCK(*clsC2*), and *clsC2* was integrated into the *A. baumannii* 17978 UN Δ*clsC2* variant by setting up a four-way mating between *E. coli λpir116*/pKNOCK(*clsC2*), *E. coli* HB101/pRK2013, *E. coli* 100D/pTNS2, and the *A. baumannii* 17978 UN Δ*clsC2* strain to make the *A. baumannii* 17978 UN Δ*clsC2*/*clsC2* strain. Successful integration of *clsC2* into the correct spot on the *A. baumannii* 17978 UN Δ*clsC2* chromosome was verified in the following two ways: first, by PCR amplification using a forward primer that binds the *A. baumannii* chromosome near the target insertion site (GTCGTTTTCGCTGATGAAAATAG) and a reverse primer that binds within the Tn*7* element (CACAGCATAACTGGACTGATTTC), and second, by PCR amplification of the *clsC2* gene inserted into the Tn*7* element.

To express *clsC2* in *trans* in *A. baumannii* 17978 VU, *clsC2* was cloned into pWH1266 as described above, using a forward primer annealing to the region upstream of *clsC2* (AACCTTCTTAGATTATAACAAAATCAT ACAGTTATTG) fused to a 20-nucleotide sequence overlapping with the BamHI-digested plasmid and a reverse primer annealing to the region downstream of *clsC2* (GCTCTCGAGAAAAAAGCAGAAG) fused to a 20-nucleotide sequence overlapping with the SalI-digested plasmid to generate pWH1266(*clsC2*). This plasmid construct (or the empty vector) was electroporated into *A. baumannii* 17978 VU as described above.

Murine infection models. All animal experiments were approved by the Vanderbilt University Medical Center (VUMC) Institutional Care and Use Committee and conformed to policies and guidelines established by VUMC, the Animal Welfare Act, the National Institutes of Health, and the American Veterinary Medical Association. Wild-type, female, 8-week-old C57BL/6 mice were purchased from

Jackson Laboratories. The murine model of *A. baumannii* pneumonia was performed as previously described (95). Briefly, *A. baumannii* was back-diluted 1:100 from overnight culture and grown in LB for 3.5 h at 37°C with constant agitation, washed twice with cold PBS, and resuspended in PBS at an appropriate cell density for infection. Mice were infected intranasally with 3×10^8 CFU of *A. baumannii* in 30 μl PBS. At 24 or 36 h postinfection (h.p.i.), mice were euthanized and organs were harvested. Lungs and spleens were homogenized, serially diluted in PBS, and plated onto LBA for bacterial enumeration. For histological analyses, lungs were inflated with 1 ml of 10% formalin, fixed, embedded, and stained as described previously (96). Mice were randomized to treatment groups using the GraphPad QuickCalcs online randomization software (https://www.graphpad.com/quickcalcs/randomize1.cfm).

Histology. Paraffin-embedded mouse tissue sections were stained with hematoxylin and eosin by the Vanderbilt University Medical Center Translational Pathology Shared Resource. Specimens were examined and imaged by K. L. Boyd, who was blind to the treatment conditions. Images are representative of at least 2 independent experiments.

Bacterial growth assays. Overnight cultures of single, isolated colonies were generated as described above. To prepare for growth assays, overnight cultures were standardized to a similar optical density at 600 nm (OD_{600}) and subsequently diluted 1:100 in 200 μl of rich medium (LB) or minimal medium (Tris minimal succinate [TMS]) in 96-well flat-bottomed tissue culture plates (Costar; Corning). Plates were incubated for 24 h at 37°C with shaking and growth was assayed by measuring OD_{600} at the indicated times using a Synergy 2 multimode reader (BioTek).

Scanning electron microscopy analyses. Bacterial cells were analyzed by scanning electron microscopy as previously described, with some modifications (97). Briefly, bacteria were cultured in LB at 37°C overnight. The following day, samples were fixed with 2.0% paraformaldehyde (Electron Microscopy Sciences) and 2.5% glutaraldehyde (Electron Microscopy Sciences) in 0.05 M sodium cacodylate (Electron Microscopy Sciences) buffer for 24 h. After primary fixation, samples were secondarily fixed in fresh 2.0% paraformaldehyde and 2.5% glutaraldehyde in 0.05 M sodium cacodylate buffer on poly-L-lysine-coated glass coverslips (Thermo Fisher) for 4 h. Samples were washed three times with 0.05 M sodium cacodylate buffer before sequential dehydration with increasing concentrations of absolute ethanol. After ethanol dehydration, samples were dried at the critical point using a critical point dryer machine (Tousimis), mounted onto aluminum SEM sample stubs (Electron Microscopy Sciences), and sputter coated with 5 nm of gold-palladium. Afterward, samples were painted with a thin strip of colloidal silver (Electron Microscopy Sciences) at the edge to facilitate charge dissipation. Bacteria were imaged with an FEI Quanta 250 field-emission gun scanning electron microscope. Micrographs shown are representative of at least four biological replicates. Pili were quantified as the fraction of cells expressing pili (no. of cells with pili/total no. of cells in each image) and the number of pili per piliated cell. At least 12 representative images of each strain were scored in a blind manner for each of four independent experiments.

Hemagglutination assay. Hemagglutination experiments were performed based on a protocol by Greene et al. (98), with modifications. *A. baumanii* 17978 VU, 17978 UN, and 17978 UN Δ*pilus* strains were grown overnight on LBA or in LB, as indicated, for 48 h at 37°C without agitation. *E. coli* UTI 89 (positive control) and *E. coli* UTI89 Δ*fimAH* (negative control) strains were grown in LB for 24 h at 37°C without agitation, diluted 1:1,000 in LB, and incubated for another 24 h at 37°C without agitation. Bacteria were normalized to an OD_{600} of 1.0, after which 1 ml of each culture was pelleted and resuspended in 100 μl of PBS. Aliquots (25 μl) of bacteria were diluted serially in wells of a 96-well U-bottomed plate containing 25 μl of PBS, after which an equal volume of a 1% suspension of washed human erythrocytes (Innovative Research, Novi, MI) was added to each well. Wells were incubated overnight at 4°C without agitation, after which the hemagglutination titer (i.e., the maximum dilution at which bacteria are able to agglutinate erythrocytes) was recorded for each strain.

Biofilm formation. Stationary-phase cultures of *A. baumanii* 17978 VU, 17978 UN, and 17978 UN Δ*pilus* strains were diluted 1:10 in LB in wells of a 96-well plate and incubated statically at 37°C for 24 to 48 h. After incubation, half of the wells were used for the determination of biomass by measuring OD_{600}, and the other half was used for the measurement of biofilm formation. Biofilm formation was determined as follows. Supernatants were aspirated from each well, cells were permeabilized with 100% ethanol (EtOH), and biofilms were stained with crystal violet solution (0.41% in 12% EtOH) for 20 min. After staining, wells were washed vigorously with PBS, and biofilms were solubilized with 33% acetic acid, after which OD_{580} was measured for each well. Biofilm formation was recorded as the ratio of biofilm to biomass (i.e., OD_{580}/OD_{600}) (99).

A549 epithelial cell adhesion assay. Immortalized human A549 epithelial cells were maintained as frozen stocks in liquid nitrogen. Prior to infection experiments, A549 cells were maintained in Dulbecco's modified Eagle medium (DMEM; Gibco, Thermo Fisher Scientific) supplemented with 10% heat-inactivated fetal bovine serum (FBS) and 1% penicillin-streptomycin (Pen-Strep). A549 cells were grown until ~75% confluence, after which they were split 1:3 in fresh medium. To prepare for infection experiments, A549 cells were seeded onto wells of 12-well plates and grown until confluence. Next, medium was aspirated from each well, and A549 cells were washed twice with prewarmed PBS. A549 cells were then infected with mid-log-phase bacteria suspended in DMEM without antibiotics at a multiplicity of infection (MOI) of 100, after which wells were incubated at 37°C for 2 h. At 2 h.p.i., medium was aspirated from each well, and nonadherent bacteria were removed by washing wells three times with PBS. A549 cells were then lysed by adding 1% Triton X-100 to each well and incubating plates at room temperature (RT) for 10 min. After lysis, 800 μl of ice-cold PBS was added to each well, and the contents of each well were pipetted up and down several times to suspend bacteria. The number of cell-associated bacteria was then determined via serial dilution in PBS and plating onto LBA. Data are represented as the percentage of cell-associated bacteria relative to that for *A. baumanii* 17978 VU.

Bacterial surface-associated motility assay. Stationary-phase cultures of *A. baumanii* 17978 VU, 17978 UN, and 17978 UN Δ*pilus* strains were washed once in LB, resuspended in LB, and standardized to a similar OD_{600} using LB as a diluent. Next, 1 μl of standardized bacterial cultures was inoculated on the surface of motility agar plates at the center. Bacterial inoculums were allowed to dry, after which plates were wrapped in parafilm and incubated overnight, upside down, single file at 37°C. After incubation, the maximum motility radius was measured.

Hydrogen peroxide susceptibility assay. *A. baumanii* 17978 VU, 17978 UN, 17978 UN Δ*katX*/EV, and 17978 UN Δ*katX*/p*katX* strains were grown to the mid-exponential phase as previously described, then inoculated into LB supplemented with 1 mM H_2O_2 at a starting inoculum of 1×10^7 CFU/ml. Bacteria were then incubated at 37°C for 30 min with constant agitation, after which the remaining number of viable bacteria was determined via serial dilution in PBS and plating onto LBA.

Total neutrophil-mediated killing (extracellular and intracellular). Neutrophil-like HL-60 cells were maintained in RPMI medium (25 mM HEPES buffer) supplemented with 10% heat-inactivated FBS and 1% Pen-Strep. Prior to infection experiments, HL-60 cells were differentiated in media supplemented with 1.3% dimethyl sulfoxide (DMSO) for 6 days. On the day of infection, differentiated HL-60 cells were seeded at a density of 1.4×10^5 to 1.8×10^5 cells/well in wells of a 96-well plate, suspended in RPMI supplemented with 0.5% heat-inactivated FBS, and incubated at 37°C for 30 min. Bacteria for the infection were prepared as follows. *A. baumanii* 17978 VU, 17978 UN, 17978 UN Δ*katX*/EV, and 17978 UN Δ*katX*/p*katX* strains were grown to the mid-log phase and washed and diluted in PBS as previously described. Prior to infection of neutrophils, bacteria were opsonized by resuspension in 20% normal human serum in RPMI and subsequent incubation at 37°C for 30 min with constant shaking at 50 rpm. Immediately following opsonization, bacteria were resuspended in RPMI supplemented with 0.5% heat-inactivated FBS and diluted further to the appropriate cell density for infection. Next, bacteria were added to each well at an MOI of 2, and the infection was synchronized by centrifuging the 96-well plate at $200 \times g$ for 9 min at 4°C. Inoculums were verified by serially diluting in PBS and plating on LBA. The plate was then incubated for 90 min at 37°C, after which infected HL-60 cells were lysed by adding saponin to a final concentration of 0.1% to each well and incubating on ice for 15 min. Next, lysates were serially diluted in PBS and plated onto LBA for bacterial enumeration.

Murine neutrophils were isolated as follows. Murine hind limbs were dissected and bone marrow was isolated as previously described (100). Briefly, bone marrow was isolated from the long bones of C57BL/6 mouse hind limbs via centrifugation, washed, red blood cells were lysed, and the bone marrow suspension was passed through a cell strainer prior to counting. Neutrophils were isolated using a mouse neutrophil isolation kit (Miltenyi Biotec) according to the manufacturer's protocol. Infection of murine neutrophils was performed as described above with modifications. Purified neutrophils were seeded at a density of 1.6×10^5 to 3.2×10^5 cells/well in wells of a 96-well plate pretreated with 100 μl of 20% normal human serum, after which they were allowed to attach to well bottoms by incubating plates at room temperature for 30 min. *A. baumanii* 17978 VU, 17978 UN, and 17978 UN Δ*katX* strains were opsonized by resuspension in 50% C57BL/6 mouse complement serum (Innovative Research, Novi, MI) in RPMI medium supplemented with 10 mM HEPES buffer (RPMI/H). Immediately following opsonization, bacteria were washed twice with RPMI/H and diluted in RPMI/H to the appropriate cell density for infection. Bacteria were added to each well at an MOI of 1 and, following synchronization of the infection, the plate was incubated for 2 h at 37°C as described above. Neutrophils were lysed and viable bacteria were enumerated as described above.

Bacterial uptake by macrophages. Immortalized macrophage-like RAW 264.7 cells were maintained as frozen stocks in liquid nitrogen. Prior to infection experiments, RAW cells were maintained in DMEM supplemented with 10% heat-inactivated FBS and 1% Pen-Strep. RAW cells were grown until ~75% confluence, after which they were split 1:10 to 1:20 in fresh medium. To prepare for infection experiments, RAW cells were seeded onto wells of 12-well plates at a seeding density of 5×10^5 cells/well and activated with 100 ng/ml of LPS, after which they were incubated overnight at 37°C. On the day of infection, mid-log-phase cultures of *A. baumannii* were prepared as previously described, after which bacteria were resuspended in DMEM plus 10% FBS devoid of antibiotics at the appropriate bacterial density to reach a target MOI of 15. Medium was then aspirated from all wells, RAW cells were washed once with prewarmed PBS, and 1 ml of appropriate bacteria suspended in medium was added to each well. Inoculums were verified by serially diluting in PBS and plating on LBA. Infected RAW cells were then incubated at 37°C for 30 min, after which medium was aspirated and wells were washed twice with prewarmed PBS. Next, extracellular bacteria were killed by adding 1 ml of medium supplemented with 200 μg/ml gentamicin to each well and incubating at 37°C. Thirty minutes after the addition of gentamicin, medium was aspirated, cells were washed once with PBS, and cells were lysed by adding 200 μl of 0.01% triton to each well. Each well was scraped with a sterile cell scraper, after which the lysate was serially diluted in PBS and plated onto LBA for the enumeration of intracellular bacterial burden.

Bacterial cell envelope stress assays. Bacterial susceptibility to osmotic stress was assayed as follows. *A. baumannii* 17978 VU, 17978 UN, 17978 UN Δ*clsC2*, and 17978 UN Δ*clsC2*/*clsC2* strains were grown to the mid-exponential phase as previously described and inoculated into LB supplemented with 2.5 M NaCl at a starting inoculum of 1×10^7 CFU/ml. Bacteria were then incubated at 37°C for 2 h with constant agitation, after which bacterial viability was determined via serial dilution in PBS and plating onto LBA. Bacterial survival was calculated as the percentage of viable bacteria postincubation relative to the number of viable bacteria preincubation. Bacterial susceptibility to detergent stress was assayed as follows. *A. baumannii* 17978 VU, 17978 UN, *A*17978 UN Δ*clsC2*, and 17978 UN Δ*clsC2*/*clsC2* strains were prepared as described above, and resuspended in PBS supplemented with 0.1% Triton X-100 at a

starting inoculum of 1×10^{10} CFU/ml. Bacteria were then incubated at 37°C for 6 h with constant agitation, after which bacterial viability and survival were determined and calculated as described above.

Detection of cytokines produced by infected macrophages. BMDMs were isolated and maintained as previously described (101). Briefly, bone marrow was isolated from the long bones of C57BL/6 mouse hind limbs via centrifugation and washed, red blood cells were lysed, and the bone marrow suspension was passed through a cell strainer prior to counting. The bone marrow cell suspension was plated at a density of 3×10^6 cells/ml in BMDM medium (RPMI medium supplemented with 10% FBS and 20% L929 cell conditioned medium [LCCM]) and incubated at 37°C with 5% CO_2. Every 48 h, medium was aspirated and fresh BMDM medium was added to each plate. On day six, BMDMs were collected and seeded onto 12-well plates at a density of 1×10^6 to 2.5×10^6 cells/well in BMDM medium and incubated overnight at 37°C. On day 7, mid-log-phase cultures of *A. baumannii* were prepared as previously described and diluted to the appropriate bacterial density in RPMI medium supplemented with 10% FBS for a target MOI of 10. Medium was then aspirated from all wells, and BMDMs were washed once with prewarmed PBS, after which bacteria suspended in 1 ml of medium were added. As a negative control, BMDMs were infected with medium alone, and as a positive control, BMDMs were treated with medium supplemented with 100 ng/ml of LPS or 100 ng/ml of LPS plus 2 mM ATP. Plates were then incubated at 37°C and the supernatant was collected at 18 h.p.i. Cytokines and chemokines (IL-1β, IL-10, KC, and MIP-2) in BMDM supernatants were quantified using an enzyme-limited immunosorbent assay (ELISA) kit (R&D Systems) according to the manufacturer's protocol for each.

Complete blood counts. Complete blood counts with five-part differential were performed on EDTA-treated whole mouse blood by the Vanderbilt University Medical Center Translational Pathology Shared Resource.

Immune cell recruitment. Flow cytometric analyses were performed with total erythrocyte-free lung cells isolated at 24 h.p.i. from individual mice infected with *A. baumannii* 17978 VU or 17978 UN variants, as indicated. Lungs were minced, digested with collagenase and DNase for 30 min, and passed through a 70-μm cell strainer prior to erythrocyte lysis. Cells were stained with a myeloid panel that included antibodies against CD45 (clone 104, fluorescein isothiocyanate [FITC]; eBioscience), CD103 (clone 2E7, PerCP-Cyanine5.5 [Cy5.5]; BioLegend), CD64 (clone X54-5/7.1, phycoerythrin [PE]; BioLegend), CD11c (clone HL-3, PE-Cy7; BD Pharmingen), Siglec F (clone E50-2440, Horizon PE-CF594; BD Pharmingen), CD11b (clone M1/70, eFluor-450; eBioscience), MHCII (clone M5/114.15.2, BV605; BD Pharmingen), CD24 (clone M1/69, allophycocyanin [APC]; eBioscience), Ly6C (clone AL-21, APC-Cy7; BD Pharmingen), and Ly6G (clone 1A8, Alexa Fluor 700; BD Pharmingen). Analyses were carried out on the 5-laser LSR Fortessa instrument (BD Biosciences) at the Vanderbilt Flow Cytometry Shared Resource, and analyses were performed using FlowJo software (Treestar, Inc.). Myeloid populations were gated according to the strategy of Misharin and colleagues (102, 103).

Quantification and statistical analysis. Statistical analyses were performed using Prism version 6 (GraphPad Software, Inc.). Mean comparisons were performed using unpaired Welch's *t* test or one-way analysis of variance (ANOVA) adjusted for multiple comparisons, as indicated. *P* values of less than 0.05 were considered statistically significant. Statistical details of the experiments can be found in the figure legends.

Data availability. The assembled genomes of *A. baumannii* 17978 VU and 17978 UN variants that were sequenced using PacBio sequencing technology are available in the NCBI database under accession numbers CP079213.1 (VU variant) and CP079212.1 (UN variant). The newly deposited reference genome of the *A. baumannii* 17978 UN variant that was sequenced using Nanopore long-read sequencing technology is available in the NCBI database under accession numbers CP079931 (chromosome), CP079932 (pAB3), CP079933 (pAB1), and CP079934 (pAB2).

SUPPLEMENTAL MATERIAL

Supplemental material is available online only.

SUPPLEMENTAL FILE 1, PDF file, 0.2 MB.

SUPPLEMENTAL FILE 2, PDF file, 2.5 MB.

ACKNOWLEDGMENTS

We thank the Vanderbilt University Medical Center (VUMC) Division of Animal Care, the VUMC Translational Pathology Shared Resource, the VUMC flow cytometry shared resource, the VUMC Molecular Cell Biology Resource Core, and the Vanderbilt Institute for Infection, Immunology, and Inflammation (VI4). Additional support for this work was provided by Padmini Komalavilas, Ph.D.

This work was funded by Cystic Fibrosis Foundation award NOTO17Q0 and National Institutes of Health award 1R01HL152210-01 to M.J.N., by National Institutes of Health Award HD090061 to J.A.G., and by National Institutes of Health award R01AI101171 to E.P.S.

REFERENCES

1. Dijkshoorn L, Nemec A, Seifert H. 2007. An increasing threat in hospitals: multidrug-resistant *Acinetobacter baumannii*. Nat Rev Microbiol 5:939–951. https://doi.org/10.1038/nrmicro1789.
2. Antunes LC, Visca P, Towner KJ. 2014. *Acinetobacter baumannii*: evolution of a global pathogen. Pathog Dis 71:292–301. https://doi.org/10.1111/2049-632X.12125.

3. Fournier PE, Richet H. 2006. The epidemiology and control of *Acinetobacter baumannii* in health care facilities. Clin Infect Dis 42:692–699. https://doi.org/10.1086/500202.
4. Inchai J, Pothirat C, Bumroongkit C, Limsukon A, Khositsakulchai W, Liwsrisakun C. 2015. Prognostic factors associated with mortality of drug-resistant *Acinetobacter baumannii* ventilator-associated pneumonia. J Intensive Care 3:9. https://doi.org/10.1186/s40560-015-0077-4.
5. Kanafani ZA, Zahreddine N, Tayyar R, Sfeir J, Araj GF, Matar GM, Kanj SS. 2018. Multi-drug resistant *Acinetobacter* species: a seven-year experience from a tertiary care center in Lebanon. Antimicrob Resist Infect Control 7:9. https://doi.org/10.1186/s13756-017-0297-6.
6. Anderson SE, Sherman EX, Weiss DS, Rather PN. 2018. Aminoglycoside heteroresistance in *Acinetobacter baumannii* AB5075. mSphere 3:e00271-18. https://doi.org/10.1128/mSphere.00271-18.
7. McGann P, Courvalin P, Snesrud E, Clifford RJ, Yoon EJ, Onmus-Leone F, Ong AC, Kwak YI, Grillot-Courvalin C, Lesho E, Waterman PE. 2014. Amplification of aminoglycoside resistance gene *aphA1* in *Acinetobacter baumannii* results in tobramycin therapy failure. mBio 5:e00915. https://doi.org/10.1128/mBio.00915-14.
8. Tada T, Miyoshi-Akiyama T, Shimada K, Shimojima M, Kirikae T. 2014. Dissemination of 16S rRNA methylase ArmA-producing *Acinetobacter baumannii* and emergence of OXA-72 carbapenemase coproducers in Japan. Antimicrob Agents Chemother 58:2916–2920. https://doi.org/10.1128/AAC.01212-13.
9. Hsu LY, Apisarnthanarak A, Khan E, Suwantarat N, Ghafur A, Tambyah PA. 2017. Carbapenem-resistant *Acinetobacter baumannii* and *Enterobacteriaceae* in South and Southeast Asia. Clin Microbiol Rev 30:1–22. https://doi.org/10.1128/CMR.00042-16.
10. Evans BA, Hamouda A, Amyes SG. 2013. The rise of carbapenem-resistant *Acinetobacter baumannii*. Curr Pharm Des 19:223–238. https://doi.org/10.2174/138161213804070285.
11. Pogue JM, Mann T, Barber KE, Kaye KS. 2013. Carbapenem-resistant *Acinetobacter baumannii*: epidemiology, surveillance and management. Expert Rev Anti Infect Ther 11:383–393. https://doi.org/10.1586/eri.13.14.
12. Tacconelli E, Carrara E, Savoldi A, Harbarth S, Mendelson M, Monnet DL, Pulcini C, Kahlmeter G, Kluytmans J, Carmeli Y, Ouellette M, Outterson K, Patel J, Cavaleri M, Cox EM, Houchens CR, Grayson ML, Hansen P, Singh N, Theuretzbacher U, Magrini N, Group W, WHO Pathogens Priority List Working Group. 2018. Discovery, research, and development of new antibiotics: the WHO priority list of antibiotic-resistant bacteria and tuberculosis. Lancet Infect Dis 18:318–327. https://doi.org/10.1016/S1473-3099(17)30753-3.
13. Park YK, Jung SI, Park KH, Cheong HS, Peck KR, Song JH, Ko KS. 2009. Independent emergence of colistin-resistant *Acinetobacter* spp. isolates from Korea. Diagn Microbiol Infect Dis 64:43–51. https://doi.org/10.1016/j.diagmicrobio.2009.01.012.
14. Dickstein Y, Lellouche J, Ben Dalak Amar M, Schwartz D, Nutman A, Daitch V, Yahav D, Leibovici L, Skiada A, Antoniadou A, Daikos GL, Andini R, Zampino R, Durante-Mangoni E, Mouton JW, Friberg LE, Dishon Benattar Y, Bitterman R, Neuberger A, Carmeli Y, Paul M, Group AS, AIDA Study Group. 2019. Treatment outcomes of colistin- and carbapenem-resistant *Acinetobacter baumannii* infections: an exploratory subgroup analysis of a randomized clinical trial. Clin Infect Dis 69:769–776. https://doi.org/10.1093/cid/ciy988.
15. Trebosc V, Gartenmann S, Tötzl M, Lucchini V, Schellhorn B, Pieren M, Lociuro S, Gitzinger M, Tigges M, Bumann D, Kemmer C. 2019. Dissecting colistin resistance mechanisms in extensively drug-resistant *Acinetobacter baumannii* clinical isolates. mBio 10:e01083-19. https://doi.org/10.1128/mBio.01083-19.
16. Li J, Nation RL, Turnidge JD, Milne RW, Coulthard K, Rayner CR, Paterson DL. 2006. Colistin: the re-emerging antibiotic for multidrug-resistant Gram-negative bacterial infections. Lancet Infect Dis 6:589–601. https://doi.org/10.1016/S1473-3099(06)70580-1.
17. Xie R, Zhang XD, Zhao Q, Peng B, Zheng J. 2018. Analysis of global prevalence of antibiotic resistance in *Acinetobacter baumannii* infections disclosed a faster increase in OECD countries. Emerg Microbes Infect 7:31. https://doi.org/10.1038/s41426-018-0038-9.
18. Hsueh PR, Teng LJ, Chen CY, Chen WH, Yu CJ, Ho SW, Luh KT. 2002. Pandrug-resistant *Acinetobacter baumannii* causing nosocomial infections in a university hospital, Taiwan. Emerg Infect Dis 8:827–832. https://doi.org/10.3201/eid0805.020014.
19. Nowak J, Zander E, Stefanik D, Higgins PG, Roca I, Vila J, McConnell MJ, Cisneros JM, Seifert H, Mwg WP4, MagicBullet Working Group WP4. 2017. High incidence of pandrug-resistant *Acinetobacter baumannii* isolates collected from patients with ventilator-associated pneumonia in Greece, Italy and Spain as part of the MagicBullet clinical trial. J Antimicrob Chemother 72:3277–3282. https://doi.org/10.1093/jac/dkx322.
20. CDC. 2019. Antibiotic resistance threats in the United States, 2019. CDC, Atlanta, GA.
21. Wright MS, Iovleva A, Jacobs MR, Bonomo RA, Adams MD. 2016. Genome dynamics of multidrug-resistant *Acinetobacter baumannii* during infection and treatment. Genome Med 8:26. https://doi.org/10.1186/s13073-016-0279-y.
22. Boone RL, Whitehead B, Avery TM, Lu J, Francis JD, Guevara MA, Moore RE, Chambers SA, Doster RS, Manning SD, Townsend SD, Dent L, Marshall D, Gaddy JA, Damo SM. 2021. Analysis of virulence phenotypes and antibiotic resistance in clinical strains of *Acinetobacter baumannii* isolated in Nashville, Tennessee. BMC Microbiol 21:21. https://doi.org/10.1186/s12866-020-02082-1.
23. Kyrpides NC, Hugenholtz P, Eisen JA, Woyke T, Göker M, Parker CT, Amann R, Beck BJ, Chain PS, Chun J, Colwell RR, Danchin A, Dawyndt P, Dedeurwaerdere T, DeLong EF, Detter JC, De Vos P, Donohue TJ, Dong XZ, Ehrlich DS, Fraser C, Gibbs R, Gilbert J, Gilna P, Glöckner FO, Jansson JK, Keasling JD, Knight R, Labeda D, Lapidus A, Lee JS, Li WJ, Ma J, Markowitz V, Moore ER, Morrison M, Meyer F, Nelson KE, Ohkuma M, Ouzounis CA, Pace N, Parkhill J, Qin N, Rossello-Mora R, Sikorski J, Smith D, Sogin M, Stevens R, Stingl U, Suzuki K, et al. 2014. Genomic encyclopedia of bacteria and archaea: sequencing a myriad of type strains. PLoS Biol 12:e1001920. https://doi.org/10.1371/journal.pbio.1001920.
24. Antunes LC, Imperi F, Carattoli A, Visca P. 2011. Deciphering the multifactorial nature of *Acinetobacter baumannii* pathogenicity. PLoS One 6:e22674. https://doi.org/10.1371/journal.pone.0022674.
25. Hugh R, Reese R. 1968. A comparison of 120 strains of *Bacterium anitratum* Schaub and Hauber with the type strain of this species. Int J Syst Evol Microbiol 18:1–3.
26. Jacobs AC, Thompson MG, Black CC, Kessler JL, Clark LP, McQueary CN, Gancz HY, Corey BW, Moon JK, Si Y, Owen MT, Hallock JD, Kwak YI, Summers A, Li CZ, Rasko DA, Penwell WF, Honnold CL, Wise MC, Waterman PE, Lesho EP, Stewart RL, Actis LA, Palys TJ, Craft DW, Zurawski DV. 2014. AB5075, a highly virulent isolate of *Acinetobacter baumannii*, as a model strain for the evaluation of pathogenesis and antimicrobial treatments. mBio 5:e01076-14–e01014. https://doi.org/10.1128/mBio.01076-14.
27. Wang N, Ozer EA, Mandel MJ, Hauser AR. 2014. Genome-wide identification of *Acinetobacter baumannii* genes necessary for persistence in the lung. mBio 5:e01163-14–e01114. https://doi.org/10.1128/mBio.01163-14.
28. Sato Y, Unno Y, Kawakami S, Ubagai T, Ono Y. 2017. Virulence characteristics of *Acinetobacter baumannii* clinical isolates vary with the expression levels of *omps*. J Med Microbiol 66:203–212. https://doi.org/10.1099/jmm.0.000394.
29. Ramirez MS, Penwell WF, Traglia GM, Zimbler DL, Gaddy JA, Nikolaidis N, Arivett BA, Adams MD, Bonomo RA, Actis LA, Tolmasky ME. 2019. Identification of potential virulence factors in the model strain *Acinetobacter baumannii* A118. Front Microbiol 10:1599. https://doi.org/10.3389/fmicb.2019.01599.
30. Hesse LE, Lonergan ZR, Beavers WN, Skaar EP. 2019. The *Acinetobacter baumannii* Znu system overcomes host-imposed nutrient zinc limitation. Infect Immun 87:e00746-19. https://doi.org/10.1128/IAI.00746-19.
31. Lonergan ZR, Nairn BL, Wang J, Hsu YP, Hesse LE, Beavers WN, Chazin WJ, Trinidad JC, VanNieuwenhze MS, Giedroc DP, Skaar EP. 2019. An *Acinetobacter baumannii*, zinc-regulated peptidase maintains cell wall integrity during immune-mediated nutrient sequestration. Cell Rep 26:2009–2018.e6. https://doi.org/10.1016/j.celrep.2019.01.089.
32. Wood CR, Ohneck EJ, Edelmann RE, Actis LA. 2018. A light-regulated type I pilus contributes to *Acinetobacter baumannii* biofilm, motility, and virulence functions. Infect Immun 86:e00442-18. https://doi.org/10.1128/IAI.00442-18.
33. Williams CL, Neu HM, Alamneh YA, Reddinger RM, Jacobs AC, Singh S, Abu-Taleb R, Michel SLJ, Zurawski DV, Merrell DS. 2020. Characterization of *Acinetobacter baumannii* copper resistance reveals a role in virulence. Front Microbiol 11:16. https://doi.org/10.3389/fmicb.2020.00016.
34. Dobrindt U, Hacker J. 2001. Whole genome plasticity in pathogenic bacteria. Curr Opin Microbiol 4:550–557. https://doi.org/10.1016/s1369-5274(00)00250-2.
35. Imperi F, Antunes LC, Blom J, Villa L, Iacono M, Visca P, Carattoli A. 2011. The genomics of *Acinetobacter baumannii*: insights into genome plasticity,

antimicrobial resistance and pathogenicity. IUBMB Life 63:1068–1074. https://doi.org/10.1002/iub.531.
36. Traglia G, Chiem K, Quinn B, Fernandez JS, Montaña S, Almuzara M, Mussi MA, Tolmasky ME, Iriarte A, Centrón D, Ramírez MS. 2018. Genome sequence analysis of an extensively drug-resistant *Acinetobacter baumannii* indigo-pigmented strain depicts evidence of increase genome plasticity. Sci Rep 8:16961. https://doi.org/10.1038/s41598-018-35377-5.
37. Liu F, Zhu Y, Yi Y, Lu N, Zhu B, Hu Y. 2014. Comparative genomic analysis of *Acinetobacter baumannii* clinical isolates reveals extensive genomic variation and diverse antibiotic resistance determinants. BMC Genomics 15:1163. https://doi.org/10.1186/1471-2164-15-1163.
38. Wright MS, Haft DH, Harkins DM, Perez F, Hujer KM, Bajaksouzian S, Benard MF, Jacobs MR, Bonomo RA, Adams MD. 2014. New insights into dissemination and variation of the health care-associated pathogen *Acinetobacter baumannii* from genomic analysis. mBio 5:e00963-13–e00913. https://doi.org/10.1128/mBio.00963-13.
39. Adams MD, Wright MS, Karichu JK, Venepally P, Fouts DE, Chan AP, Richter SS, Jacobs MR, Bonomo RA. 2019. Rapid replacement of *Acinetobacter baumannii* strains accompanied by changes in lipooligosaccharide loci and resistance gene repertoire. mBio 10:e00356-19. https://doi.org/10.1128/mBio.00356-19.
40. Jaidane N, Naas T, Mansour W, Radhia BB, Jerbi S, Boujaafar N, Bouallegue O, Bonnin RA. 2018. Genomic analysis of *in vivo* acquired resistance to colistin and rifampicin in *Acinetobacter baumannii*. Int J Antimicrob Agents 51:266–269. https://doi.org/10.1016/j.ijantimicag.2017.10.016.
41. Talyansky Y, Nielsen TB, Yan J, Carlino-Macdonald U, Di Venanzio G, Chakravorty S, Ulhaq A, Feldman MF, Russo TA, Vinogradov E, Luna B, Wright MS, Adams MD, Spellberg B. 2021. Capsule carbohydrate structure determines virulence in *Acinetobacter baumannii*. PLoS Pathog 17:e1009291. https://doi.org/10.1371/journal.ppat.1009291.
42. Weber BS, Ly PM, Irwin JN, Pukatzki S, Feldman MF. 2015. A multidrug resistance plasmid contains the molecular switch for type VI secretion in *Acinetobacter baumannii*. Proc Natl Acad Sci U S A 112:9442–9447. https://doi.org/10.1073/pnas.1502966112.
43. Weber BS, Miyata ST, Iwashkiw JA, Mortensen BL, Skaar EP, Pukatzki S, Feldman MF. 2013. Genomic and functional analysis of the type VI secretion system in *Acinetobacter*. PLoS One 8:e55142. https://doi.org/10.1371/journal.pone.0055142.
44. Kim J, Lee JY, Lee H, Choi JY, Kim DH, Wi YM, Peck KR, Ko KS. 2017. Microbiological features and clinical impact of the type VI secretion system (T6SS) in *Acinetobacter baumannii* isolates causing bacteremia. Virulence 8:1378–1389. https://doi.org/10.1080/21505594.2017.1323164.
45. Jensen T, Tellgren-Roth C, Redl S, Maury J, Jacobsen SAB, Pedersen LE, Nielsen AT. 2019. Genome-wide systematic identification of methyltransferase recognition and modification patterns. Nat Commun 10:3311. https://doi.org/10.1038/s41467-019-11179-9.
46. Breslow JM, Meissler JJ, Hartzell RR, Spence PB, Truant A, Gaughan J, Eisenstein TK. 2011. Innate immune responses to systemic *Acinetobacter baumannii* infection in mice: neutrophils, but not interleukin-17, mediate host resistance. Infect Immun 79:3317–3327. https://doi.org/10.1128/IAI.00069-11.
47. van Faassen H, KuoLee R, Harris G, Zhao X, Conlan JW, Chen W. 2007. Neutrophils play an important role in host resistance to respiratory infection with *Acinetobacter baumannii* in mice. Infect Immun 75:5597–5608. https://doi.org/10.1128/IAI.00762-07.
48. Qiu H, KuoLee R, Harris G, Chen W. 2009. High susceptibility to respiratory *Acinetobacter baumannii* infection in A/J mice is associated with a delay in early pulmonary recruitment of neutrophils. Microbes Infect 11:946–955. https://doi.org/10.1016/j.micinf.2009.06.003.
49. Mahmutovic Persson I, Menzel M, Ramu S, Cerps S, Akbarshahi H, Uller L. 2018. IL-1β mediates lung neutrophilia and IL-33 expression in a mouse model of viral-induced asthma exacerbation. Respir Res 19:16. https://doi.org/10.1186/s12931-018-0725-z.
50. Miller LS, Pietras EM, Uricchio LH, Hirano K, Rao S, Lin H, O'Connell RM, Iwakura Y, Cheung AL, Cheng G, Modlin RL. 2007. Inflammasome-mediated production of IL-1β is required for neutrophil recruitment against *Staphylococcus aureus in vivo*. J Immunol 179:6933–6942. https://doi.org/10.4049/jimmunol.179.10.6933.
51. Biondo C, Mancuso G, Midiri A, Signorino G, Domina M, Lanza Cariccio V, Mohammadi N, Venza M, Venza I, Teti G, Beninati C. 2014. The interleukin-1β/CXCL1/2/neutrophil axis mediates host protection against group B streptococcal infection. Infect Immun 82:4508–4517. https://doi.org/10.1128/IAI.02104-14.
52. Mantovani A, Dinarello CA, Molgora M, Garlanda C. 2019. Interleukin-1 and related cytokines in the regulation of inflammation and immunity. Immunity 50:778–795. https://doi.org/10.1016/j.immuni.2019.03.012.
53. Andrade EB, Alves J, Madureira P, Oliveira L, Ribeiro A, Cordeiro-da-Silva A, Correia-Neves M, Trieu-Cuot P, Ferreira P. 2013. TLR2-induced IL-10 production impairs neutrophil recruitment to infected tissues during neonatal bacterial sepsis. J Immunol 191:4759–4768. https://doi.org/10.4049/jimmunol.1301752.
54. Sun L, Guo RF, Newstead MW, Standiford TJ, Macariola DR, Shanley TP. 2009. Effect of IL-10 on neutrophil recruitment and survival after *Pseudomonas aeruginosa* challenge. Am J Respir Cell Mol Biol 41:76–84. https://doi.org/10.1165/rcmb.2008-0202OC.
55. Tucker AT, Nowicki EM, Boll JM, Knauf GA, Burdis NC, Trent MS, Davies BW. 2014. Defining gene-phenotype relationships in *Acinetobacter baumannii* through one-step chromosomal gene inactivation. mBio 5:e01313-14–e01314. https://doi.org/10.1128/mBio.01313-14.
56. Avalos Vizcarra I, Hosseini V, Kollmannsberger P, Meier S, Weber SS, Arnoldini M, Ackermann M, Vogel V. 2016. How type 1 fimbriae help *Escherichia coli* to evade extracellular antibiotics. Sci Rep 6:18109. https://doi.org/10.1038/srep18109.
57. Lo AW, Van de Water K, Gane PJ, Chan AW, Steadman D, Stevens K, Selwood DL, Waksman G, Remaut H. 2014. Suppression of type 1 pilus assembly in uropathogenic *Escherichia coli* by chemical inhibition of subunit polymerization. J Antimicrob Chemother 69:1017–1026. https://doi.org/10.1093/jac/dkt467.
58. Martinez JJ, Mulvey MA, Schilling JD, Pinkner JS, Hultgren SJ. 2000. Type 1 pilus-mediated bacterial invasion of bladder epithelial cells. EMBO J 19:2803–2812. https://doi.org/10.1093/emboj/19.12.2803.
59. Sarkar S, Vagenas D, Schembri MA, Totsika M. 2016. Biofilm formation by multidrug resistant *Escherichia coli* ST131 is dependent on type 1 fimbriae and assay conditions. Pathog Dis 74: ftw013. https://doi.org/10.1093/femspd/ftw013.
60. Imlay JA. 2013. The molecular mechanisms and physiological consequences of oxidative stress: lessons from a model bacterium. Nat Rev Microbiol 11:443–454. https://doi.org/10.1038/nrmicro3032.
61. Wan B, Zhang Q, Ni J, Li S, Wen D, Li J, Xiao H, He P, Ou HY, Tao J, Teng Q, Lu J, Wu W, Yao YF. 2017. Type VI secretion system contributes to enterohemorrhagic *Escherichia coli* virulence by secreting catalase against host reactive oxygen species (ROS). PLoS Pathog 13:e1006246. https://doi.org/10.1371/journal.ppat.1006246.
62. Goulart CL, Barbosa LC, Bisch PM, von Krüger WMA. 2016. Catalases and PhoB/PhoR system independently contribute to oxidative stress resistance in *Vibrio cholerae* O1. Microbiology (Reading) 162:1955–1962. https://doi.org/10.1099/mic.0.000364.
63. El-Benna J, Hurtado-Nedelec M, Marzaioli V, Marie JC, Gougerot-Pocidalo MA, Dang PM. 2016. Priming of the neutrophil respiratory burst: role in host defense and inflammation. Immunol Rev 273:180–193. https://doi.org/10.1111/imr.12447.
64. Nguyen GT, Green ER, Mecsas J. 2017. Neutrophils to the ROScue: mechanisms of NADPH oxidase activation and bacterial resistance. Front Cell Infect Microbiol 7:373. https://doi.org/10.3389/fcimb.2017.00373.
65. Tropp BE. 1997. Cardiolipin synthase from *Escherichia coli*. Biochim Biophys Acta 1348:192–200. https://doi.org/10.1016/s0005-2760(97)00100-8.
66. Tan BK, Bogdanov M, Zhao J, Dowhan W, Raetz CR, Guan Z. 2012. Discovery of a cardiolipin synthase utilizing phosphatidylethanolamine and phosphatidylglycerol as substrates. Proc Natl Acad Sci U S A 109:16504–16509. https://doi.org/10.1073/pnas.1212797109.
67. Renner LD, Weibel DB. 2011. Cardiolipin microdomains localize to negatively curved regions of *Escherichia coli* membranes. Proc Natl Acad Sci U S A 108:6264–6269. https://doi.org/10.1073/pnas.1015757108.
68. Rowlett VW, Mallampalli VKPS, Karlstaedt A, Dowhan W, Taegtmeyer H, Margolin W, Vitrac H. 2017. Impact of membrane phospholipid alterations in *Escherichia coli* on cellular function and bacterial stress adaptation. J Bacteriol 199 :e00849-16. https://doi.org/10.1128/JB.00849-16.
69. López CS, Alice AF, Heras H, Rivas EA, Sánchez-Rivas C. 2006. Role of anionic phospholipids in the adaptation of *Bacillus subtilis* to high salinity. Microbiology (Reading) 152:605–616. https://doi.org/10.1099/mic.0.28345-0.
70. López GA, Heredia RM, Boeris PS, Lucchesi GI. 2016. Content of cardiolipin of the membrane and sensitivity to cationic surfactants in *Pseudomonas putida*. J Appl Microbiol 121:1004–1014. https://doi.org/10.1111/jam.13238.
71. Balasubramanian K, Maeda A, Lee JS, Mohammadyani D, Dar HH, Jiang JF, St Croix CM, Watkins S, Tyurin VA, Tyurina YY, Klöditz K, Polimova A, Kapralova VI, Xiong Z, Ray P, Klein-Seetharaman J, Mallampalli RK, Bayir

H, Fadeel B, Kagan VE. 2015. Dichotomous roles for externalized cardiolipin in extracellular signaling: promotion of phagocytosis and attenuation of innate immunity. Sci Signal 8:ra95. https://doi.org/10.1126/scisignal.aaa6179.
72. Iyer SS, He Q, Janczy JR, Elliott EI, Zhong Z, Olivier AK, Sadler JJ, Knepper-Adrian V, Han R, Qiao L, Eisenbarth SC, Nauseef WM, Cassel SL, Sutterwala FS. 2013. Mitochondrial cardiolipin is required for Nlrp3 inflammasome activation. Immunity 39:311–323. https://doi.org/10.1016/j.immuni.2013.08.001.
73. Pizzuto M, Lonez C, Baroja-Mazo A, Martínez-Banaclocha H, Tourlomousis P, Gangloff M, Pelegrin P, Ruysschaert JM, Gay NJ, Bryant CE. 2019. Saturation of acyl chains converts cardiolipin from an antagonist to an activator of Toll-like receptor-4. Cell Mol Life Sci 76:3667–3678. https://doi.org/10.1007/s00018-019-03113-5.
74. Sahl JW, Gillece JD, Schupp JM, Waddell VG, Driebe EM, Engelthaler DM, Keim P. 2013. Evolution of a pathogen: a comparative genomics analysis identifies a genetic pathway to pathogenesis in *Acinetobacter*. PLoS One 8:e54287. https://doi.org/10.1371/journal.pone.0054287.
75. Klockgether J, Munder A, Neugebauer J, Davenport CF, Stanke F, Larbig KD, Heeb S, Schöck U, Pohl TM, Wiehlmann L, Tümmler B. 2010. Genome diversity of *Pseudomonas aeruginosa* PAO1 laboratory strains. J Bacteriol 192:1113–1121. https://doi.org/10.1128/JB.01515-09.
76. Monteford J, Bilverstone TW, Ingle P, Philip S, Kuehne SA, Minton NP. 2021. What's a SNP between friends: the lineage of *Clostridioides difficile* R20291 can effect research outcomes. Anaerobe 71:102422. https://doi.org/10.1016/j.anaerobe.2021.102422.
77. Juttukonda LJ, Green ER, Lonergan ZR, Heffern MC, Chang CJ, Skaar EP. 2019. OxyR regulates the transcriptional response to hydrogen peroxide. Infect Immun 87:e00413-18. https://doi.org/10.1128/IAI.00413-18.
78. Palmer LD, Minor KE, Mettlach JA, Rivera ES, Boyd KL, Caprioli RM, Spraggins JM, Dalebroux ZD, Skaar EP. 2020. Modulating isoprenoid biosynthesis increases lipooligosaccharides and restores *Acinetobacter baumannii* resistance to host and antibiotic stress. Cell Rep 32:108129. https://doi.org/10.1016/j.celrep.2020.108129.
79. Chakraborty K, Raundhal M, Chen BB, Morse C, Tyurina YY, Khare A, Oriss TB, Huff R, Lee JS, St Croix CM, Watkins S, Mallampalli RK, Kagan VE, Ray A, Ray P. 2017. The mito-DAMP cardiolipin blocks IL-10 production causing persistent inflammation during bacterial pneumonia. Nat Commun 8:13944. https://doi.org/10.1038/ncomms13944.
80. Garg M, Johri S, Sagar S, Mundhada A, Agrawal A, Ray P, Chakraborty K. 2021. Cardiolipin-mediated PPARγ S112 phosphorylation impairs IL-10 production and inflammation resolution during bacterial pneumonia. Cell Rep 34:108736. https://doi.org/10.1016/j.celrep.2021.108736.
81. Saraiva M, O'Garra A. 2010. The regulation of IL-10 production by immune cells. Nat Rev Immunol 10:170–181. https://doi.org/10.1038/nri2711.
82. Moreira LO, El Kasmi KC, Smith AM, Finkelstein D, Fillon S, Kim YG, Núñez G, Tuomanen E, Murray PJ. 2008. The TLR2-MyD88-NOD2-RIPK2 signalling axis regulates a balanced pro-inflammatory and IL-10-mediated anti-inflammatory cytokine response to Gram-positive cell walls. Cell Microbiol 10:2067–2077. https://doi.org/10.1111/j.1462-5822.2008.01189.x.
83. Castro F, Cardoso AP, Gonçalves RM, Serre K, Oliveira MJ. 2018. Interferon-gamma at the crossroads of tumor immune surveillance or evasion. Front Immunol 9:847. https://doi.org/10.3389/fimmu.2018.00847.
84. Darwich L, Coma G, Peña R, Bellido R, Blanco EJ, Este JA, Borras FE, Clotet B, Ruiz L, Rosell A, Andreo F, Parkhouse RM, Bofill M. 2009. Secretion of interferon-γ by human macrophages demonstrated at the single-cell level after costimulation with interleukin (IL)-12 plus IL-18. Immunology 126:386–393. https://doi.org/10.1111/j.1365-2567.2008.02905.x.
85. Robinson CM, O'Dee D, Hamilton T, Nau GJ. 2010. Cytokines involved in interferon-γ production by human macrophages. J Innate Immun 2:56–65. https://doi.org/10.1159/000247156.
86. Sun D, Crowell SA, Harding CM, De Silva PM, Harrison A, Fernando DM, Mason KM, Santana E, Loewen PC, Kumar A, Liu Y. 2016. KatG and KatE confer *Acinetobacter* resistance to hydrogen peroxide but sensitize bacteria to killing by phagocytic respiratory burst. Life Sci 148:31–40. https://doi.org/10.1016/j.lfs.2016.02.015.
87. Wright MS, Mountain S, Beeri K, Adams MD. 2017. Assessment of insertion sequence mobilization as an adaptive response to oxidative stress in *Acinetobacter baumannii* using IS-seq. J Bacteriol 199:e00833-16. https://doi.org/10.1128/JB.00833-16.
88. Pfefferle K, Lopalco P, Breisch J, Siemund A, Corcelli A, Averhoff B. 2020. *In vivo* synthesis of monolysocardiolipin and cardiolipin by *Acinetobacter baumannii* phospholipase D and effect on cationic antimicrobial peptide resistance. Environ Microbiol 22:5300–5308. https://doi.org/10.1111/1462-2920.15231.
89. Lopalco P, Stahl J, Annese C, Averhoff B, Corcelli A. 2017. Identification of unique cardiolipin and monolysocardiolipin species in *Acinetobacter baumannii*. Sci Rep 7:2972. https://doi.org/10.1038/s41598-017-03214-w.
90. Boyd KJ, Alder NN, May ER. 2018. Molecular dynamics analysis of cardiolipin and monolysocardiolipin on bilayer properties. Biophys J 114:2116–2127. https://doi.org/10.1016/j.bpj.2018.04.001.
91. Powers MJ, Simpson BW, Trent MS. 2020. The Mla pathway in *Acinetobacter baumannii* has no demonstrable role in anterograde lipid transport. Elife 9:e56571. https://doi.org/10.7554/eLife.56571.
92. Deatherage DE, Barrick JE. 2014. Identification of mutations in laboratory-evolved microbes from next-generation sequencing data using breseq. Methods Mol Biol 1151:165–188. https://doi.org/10.1007/978-1-4939-0554-6_12.
93. Barrick JE, Colburn G, Deatherage DE, Traverse CC, Strand MD, Borges JJ, Knoester DB, Reba A, Meyer AG. 2014. Identifying structural variation in haploid microbial genomes from short-read resequencing data using breseq. BMC Genomics 15:1039. https://doi.org/10.1186/1471-2164-15-1039.
94. Kumar A, Dalton C, Cortez-Cordova J, Schweizer HP. 2010. Mini-Tn*7* vectors as genetic tools for single copy gene cloning in *Acinetobacter baumannii*. J Microbiol Methods 82:296–300. https://doi.org/10.1016/j.mimet.2010.07.002.
95. Hood MI, Mortensen BL, Moore JL, Zhang Y, Kehl-Fie TE, Sugitani N, Chazin WJ, Caprioli RM, Skaar EP. 2012. Identification of an *Acinetobacter baumannii* zinc acquisition system that facilitates resistance to calprotectin-mediated zinc sequestration. PLoS Pathog 8:e1003068. https://doi.org/10.1371/journal.ppat.1003068.
96. Jacobs AC, Hood I, Boyd KL, Olson PD, Morrison JM, Carson S, Sayood K, Iwen PC, Skaar EP, Dunman PM. 2010. Inactivation of phospholipase D diminishes *Acinetobacter baumannii* pathogenesis. Infect Immun 78:1952–1962. https://doi.org/10.1128/IAI.00889-09.
97. Gaddy JA, Tomaras AP, Actis LA. 2009. The *Acinetobacter baumannii* 19606 OmpA protein plays a role in biofilm formation on abiotic surfaces and in the interaction of this pathogen with eukaryotic cells. Infect Immun 77:3150–3160. https://doi.org/10.1128/IAI.00096-09.
98. Greene SE, Hibbing ME, Janetka J, Chen SL, Hultgren SJ. 2015. Human urine decreases function and expression of type 1 pili in uropathogenic *Escherichia coli*. mBio 6:e00820. https://doi.org/10.1128/mBio.00820-15.
99. Álvarez-Fraga L, Pérez A, Rumbo-Feal S, Merino M, Vallejo JA, Ohneck EJ, Edelmann RE, Beceiro A, Vázquez-Ucha JC, Valle J, Actis LA, Bou G, Poza M. 2016. Analysis of the role of the LH92_11085 gene of a biofilm hyperproducing *Acinetobacter baumannii* strain on biofilm formation and attachment to eukaryotic cells. Virulence 7:443–455. https://doi.org/10.1080/21505594.2016.1145335.
100. Amend SR, Valkenburg KC, Pienta KJ. 2016. Murine hind limb long bone dissection and bone marrow isolation. J Vis Exp (110):53936. https://doi.org/10.3791/53936.
101. Zhang X, Goncalves R, Mosser DM. 2008. The isolation and characterization of murine macrophages. Curr Protoc Immunol Chapter 14:Unit 14.1.
102. Hood-Pishchany MI, Pham L, Wijers CD, Burns WJ, Boyd KL, Palmer LD, Skaar EP, Noto MJ. 2020. Broad-spectrum suppression of bacterial pneumonia by aminoglycoside-propagated *Acinetobacter baumannii*. PLoS Pathog 16:e1008374. https://doi.org/10.1371/journal.ppat.1008374.
103. Misharin AV, Morales-Nebreda L, Mutlu GM, Budinger GR, Perlman H. 2013. Flow cytometric analysis of macrophages and dendritic cell subsets in the mouse lung. Am J Respir Cell Mol Biol 49:503–510. https://doi.org/10.1165/rcmb.2013-0086MA.
104. Smith MG, Gianoulis TA, Pukatzki S, Mekalanos JJ, Ornston LN, Gerstein M, Snyder M. 2007. New insights into *Acinetobacter baumannii* pathogenesis revealed by high-density pyrosequencing and transposon mutagenesis. Genes Dev 21:601–614. https://doi.org/10.1101/gad.1510307.